ASSESSMENT OF THE MIXING STATE AND CLOUD NUCLEATING EFFICIENCY OF ASIAN AEROSOLS USING AIRCRAFT-BASED MEASUREMENTS OF HYGROSCOPICITY

A Thesis

by

TIMOTHY WILLIAM THOMAS

Submitted to the Office of Graduate Studies of
Texas A&M University
in partial fulfillment of the requirements for the degree of

MASTER OF SCIENCE

May 2006

Major Subject: Atmospheric Sciences

ASSESSMENT OF THE MIXING STATE AND CLOUD NUCLEATING EFFICIENCY OF ASIAN AEROSOLS USING AIRCRAFT-BASED MEASUREMENTS OF HYGROSCOPICITY

A Thesis

by

TIMOTHY WILLIAM THOMAS

Submitted to the Office of Graduate Studies of
Texas A&M University
in partial fulfillment of the requirements for the degree of

MASTER OF SCIENCE

Approved by:

Chair of Committee,	Donald Collins
Committee Members,	Renyi Zhang
	William Marlow
Head of Department,	Richard E. Orville

May 2006

Major Subject: Atmospheric Sciences

ABSTRACT

Assessment of the Mixing State and Cloud Nucleating Efficiency of Asian Aerosols Using Aircraft-Based Measurements of Hygroscopicity. (May 2006)

Timothy William Thomas, B.S., State University of New York at Oswego

Chair of Advisory Committee: Dr. Don Collins

Global warming theories continue to overestimate their predictions of increased mean global temperatures (Hudson 1991). This would imply that some other influence is counteracting the global warming influences; i.e. a cooling effect. Cloud albedo characteristics are currently being researched to determine the impact clouds have on the net cooling of the atmosphere in relation to the global warming theory. These characteristics are influenced by the type, size, composition, and abundance of aerosol particles that act as cloud condensation nuclei. This study employs Tandem Differential Mobility Analyzer (TDMA) data collected in the vicinity of Japan during the Asian Aerosol Characterization Experiment (ACE-Asia) to investigate the influence of aerosol concentration and composition on the light scattering properties of clouds. Measurements of particle size (Dp), particle growth factor (GF), and relative humidity (RH) yield critical supersaturations (Sc) with the assumption that the soluble part of the particle is composed primarily of one substance. This indirect composition analysis allows us to determine whether the aerosol was internally mixed (particles have uniform composition and yield a single-peak distribution or similar growth factors) or externally

mixed (different particles have different compositions yielding multiple peaks in the distribution). Through the use of calculated supersaturations, we can gain insight into cloud droplet activation properties of the samples for various aerosol types, which ultimately allows us to look at the influence of these particles on albedo characteristics of clouds formed by these particles.

DEDICATION

To my loving wife for her sacrifices and encouragement

and

my parents for their continued support.

ACKNOWLEDGMENTS

There are a few people I would like to thank for their part in helping me complete my master's degree. First, I would like to thank my parents and other family members for their continued support and encouragement. Second, this work would not have been possible had I not worked under such a great professor. Dr. Don Collins took me under his wing and introduced me to the world of aerosol research, giving me the opportunity to complete my master's. If it wasn't for his support and patience, I would not have the rewarding teaching career in New York that I do today. I would also like to acknowledge my other thesis committee members, Drs. Bill Marlow and Renyi Zhang, for their continued support and guidance. Third, I would like to thank my many colleagues, office staff, other atmospheric science professors, and friends that offered help and support all along the way, especially Scott Steiger, Brandon Ely, and Roberto Gasparini.

Lastly, I would like to acknowledge my loving and beautiful wife Jenni - my inspiration and motivation for living life to the fullest and making me who I am today. Thank you for your ongoing support and encouragement all along the way!

TABLE OF CONTENTS

Page

1. INTRODUCTION

The study of aerosols and their effects on atmospheric processes (like cloud activation, cloud droplet formation, droplet growth, and light scattering properties) continues to gain more interest as the magnitudes of these effects are identified. The need for understanding aerosol properties also continues to increase due to phenomena like climate change and regional air pollution. Only through vast research efforts will we be able to quantify the magnitude of the effects aerosols have on these phenomena and identify possible solutions. Aerosol research studies aimed at investigating influences on cloud properties typically focus on aerosol particles in the sub-micrometer range since these dominate the concentration of those particles, called cloud condensation nuclei, that can activate to form cloud droplets. Although larger particles are typically too dilute to influence cloud microphysics, they may alter the Earth's radiation budget directly through scattering and absorption of sunlight.

Cloud condensation nuclei (CCN) concentrations are typically measured by exposing an aerosol to a controlled supersaturation and then counting those particles that grow to cloud droplet size. Although this is a direct measure of CCN, it does not permit rapid characterization of the spectrum of critical supersaturations within an aerosol population. The approach taken here uses measurement of hygroscopic growth under

---

This thesis follows the style of *Monthly Weather Review*.

subsaturated conditions to infer critical supersaturation. Specifically, the ratio of the hydrated size of a particle to its dry size (growth factor or GF) is combined with Köhler Theory to predict activation properties.

A common approach to analyzing and/or modeling aerosols is to assume that aerosol particles are perfectly round spheres composed of an insoluble core surrounded by a uniform substance, generally a salt solution (Svenningsson et al. 1992). However, studies have shown that individual aerosol particles are composed of multiple species (Quinn et al. 2000, Raymond & Pandis 2003), and are often non-spherical (Crouzet and Marlow 1995). The justification for the simplification has been the assumption that the effects of irregular shape and non-uniform composition are negligible. However, Svenningson et al. (1992) have shown that these effects do have a significant role in determining cloud droplet activation properties for particles on the order of a micron in size. In addition, Crouzet & Marlow (1995) showed that curvature effects associated with adhering primary particles may alter equilibrium vapor pressure sufficiently to enable activation of less soluble non-spherical particles at atmospheric supersaturations. These studies further demonstrate the importance of aerosol irregularities.

Quinn et al. (2000) used data from the first and second Aerosol Characterization Experiments (ACE-1 and ACE-2) to study aerosol chemical and optical properties, where not only did they find impacts on albedo by continental sources when the air sampled traversed over land areas, but they also found continental influences during marine flow episodes. Collins et al. (2000) also collected data during ACE-2 and categorized the boundary layer aerosols as either continentally-influenced or maritime,

and the free tropospheric aerosols based on dust loading. Hudson (1991), Twomey (1991), Facchini et al. (1999) and Ackerman et al. (2000) also linked CCN attributed to anthropogenic sources to radiation effects, also referred to as 'indirect aerosol effects'. The common conclusion from these studies is that this effect on cloud albedo is counteracting global warming, which would help to explain the shortfall of previous projected global temperature increases (Hudson 1991).

One of the current methods for sampling submicrometer particles is humidified tandem differential mobility analysis (HTDMA). An HTDMA system (see Figure 3) is comprised of two differential mobility analyzers (DMA's) linked in series with an RH-controlled interface between them. Each DMA separates particles as a function of their electrical mobility. This process begins with passing a dried polydisperse aerosol sample through the first DMA, which is set to collect a specific dry particle size. This yields a quasi-monodisperse aerosol at the exit of the first DMA, where the aerosol can either be directed to the condensation nucleus counter (CNC), where the particles are counted as a quasi-monodisperse sample, or the aerosol can be directed through a nafion tube bundle with a prescribed RH. This exposes the quasi-monodisperse aerosol to a humidified environment where the hygroscopic aerosol particles experience hygroscopic growth and the hydrophobic particles will not. The result is a polydisperse aerosol as a function of hygroscopicity that is then passed through the second DMA, which scans across the sizes by ramping the voltage up and then down to complete one scan. As the DMA scans, the exiting aerosol is passed to the CNC and then exits the system. The

growth factor of the particles can then be determined using the ratio of the humidified particle size to the dry particle size.

Previous studies have used this technique to study hygroscopic properties of aerosol particles (Swietlicki et al. 2000) and to estimate critical supersaturation of quasi-monodisperse, dry particles (Brechtel and Kreidenweis 2000a; Brechtel and Kreidenweis 2000b). Both of these studies by Brechtel and Kreidenweis used direct measurements of aerosol hygroscopicity to infer cloud droplet activation properties. Inferred CCN concentrations can then be used in the analysis of differential changes in cloud droplet concentrations causing changes in cloud albedo (Twomey 1991) and the effects of aerosols on cloud albedo (Toon et al. 2000).

This study employs Tandem Differential Mobility Analyzer (TDMA) data collected in the vicinity of Japan during the Asian Aerosol Characterization Experiment (ACE-Asia) to investigate the influence of aerosol concentration and composition on the optical properties of clouds. Measurements of particle size (Dp), particle growth factor (GF), and relative humidity (RH) yield critical supersaturations (Sc) with the assumption that the soluble portion of the particle is composed entirely of one substance. This indirect composition analysis also allows us to infer the mixing state of the aerosol.

An internally mixed aerosol contains particles that have uniform composition while an externally mixed aerosol contains multiple particle types, each of which is composed of a single component (See Figure 1). Various atmospheric properties, such as the scattering and absorption efficiencies of the aerosol, are sensitive to the aerosol mixing state. According to Seinfeld and Pandis (1998), if the two mixing states for an

aerosol containing soot and $(NH_4)_2SO_4$ are considered, the external mixture has a higher scattering coefficient and the internal mixture has a higher absorption coefficient. Growth factor distributions clearly reflect size-dependent mixing state when hygroscopic and hydrophobic components are present. Through the use of calculated supersaturations, cloud droplet activation properties of the samples for various aerosol types, and the influences of these particles on cloud albedo, can be acquired.

2. RESEARCH METHOD AND PROCEDURE

2.1. Köhler Theory

In this study, Köhler Theory is used to extrapolate measurements of hygroscopicity under subsaturated conditions to particle activation properties. The Köhler Equation combines the Kelvin Effect (which describes an increase in vapor pressure over a droplet relative to that over a flat surface) and the solute effect (which describes a decrease in vapor pressure over a solution droplet relative to that over pure water). The following form of the Köhler Equation is used:

$$\ln\left(\frac{p_w(D_p)}{p^o}\right) = \frac{4M_w\sigma_w}{RT\rho_w D_p} + \ln\gamma_w - \ln\left(1 + \frac{n_s \bar{v}_w}{(\pi/6)D_p^3 - n_s \bar{v}_s}\right) \quad (1)$$

where $P_w(D_p)$ is the water vapor pressure over a solution droplet of diameter D_p, p^o is the water vapor pressure over a flat surface, M_w is the molecular weight of water, σ_w is the surface tension of the air-solution interface, R is the universal gas constant, T is the absolute temperature, ρ_w is the water density, γ_w is the activity coefficient of water in the solution, n_s represents the number of moles of solute, and $\bar{v}_w$ and $\bar{v}_s$ are the molar volumes of the water and salt species, respectively. The empirical polynomial coefficients from Tang and Munkelwitz (1994), Tang (1996), and Tang et al. (1997) are used to calculate water activity and solution density of the various inorganic compounds considered. These values are given in Table 1. With these empirical coefficients, activity, a_w, is related to solute weight percent, x^i, through

$$a_w = 1.0 + \sum C_i x^i \quad (2)$$

and solution density, d, is calculated in a similar manner using

$$d = 0.9971 + \sum A_i x^i \tag{3}$$

where C_i and A_i are the corresponding polynomial coefficients from Table 1.

For dilute solutions,

$$n_s \bar{v}_s << \frac{\pi}{6} D_p^3 \tag{4}$$

and the volume of the solute can be neglected. This approximation leads to the final form of the equation used:

$$\ln\left(\frac{p_w(D_p)}{p^o}\right) = \frac{4M_w\sigma_w}{RT\rho_w D_p} + \ln\gamma_w - \ln\left(1 + \frac{6n_s \bar{v}_w}{\pi D_p^3}\right) \tag{5}$$

Iterative solution of this equation for the compounds in Table 1 (see Figure 2), is used to create data tables containing the critical supersaturations corresponding to a given RH, and GF for particles with dry diameters, Dp, of 0.040 μm, 0.059 μm, 0.086 μm, 0.126 μm, 0.186 μm, 0.273 μm, and 0.400 μm. In creating these tables, particles that are composed of an inorganic part (i.e. hygroscopic salts) and a hydrophobic part (i.e. dust) are considered first. Using Köhler Theory, critical supersaturations are produced for the observed range in hygroscopicity. For small growth factors, all of the species included in Table 1 are considered; as the growth factor increases, only the subset of the species (while in their pure state) capable of resulting in the specified growth factor are considered. This can potentially constrain the composition from the observed growth of the particles.

2.2. Calculation of Critical Supersaturations

Critical supersaturations are calculated for those mixtures that are capable of representing the hygroscopic growth are compiled into three data tables: One with the maximum possible critical supersaturations, one with the minimum possible critical supersaturations, and one with the average supersaturation of mixtures containing the subset of compounds for which the pure-inorganic hygroscopicity exceeded that measured (see Tables 2 through 4). This yields data tables for all the possible critical supersaturations for each dry particle size, for a given growth factor ranging from 1 to 2.5, consistent with the species considered and the RH employed with values ranging from 80% to 96%. These data tables are used in conjunction with the aerosol data acquired during ACE-Asia to create distributions of differential number concentration versus critical supersaturation (dN/dlogSc vs. Sc). Linear interpolation onto uniformly spaced critical supersaturation bins is performed in order to compare distributions.

2.3. Data and Instrumentation

The data used for this study were collected using the system depicted in Figure 3. This system was mounted on the Center for Interdisciplinary Remotely Piloted Aircraft Studies (CIRPAS) twin otter aircraft used during the Aerosol Characterization Experiment-Asia (ACE-Asia) during April and May of 2001. Traverses were taken in the vicinity of, and areas south of, Japan. The measurements were classified into three groups based on sampling altitude: Below 300 m, between 300 m and 2000 m, and above 2000 m (see Table 5). The data are grouped in this manner to isolate the properties of the boundary layer aerosol (<300 m), the free tropospheric aerosol

(> 2000 m), and the frequent pollution layer aerosol that resided in between these extremes. The main components of the sampling system used include two Aerosol Dynamics, Inc. High Flow DMAs, two Nafion tubes, a condensation particle counter (CPC), and a computer. The High Flow DMAs are used in the system to maximize the count rate since they sample at a flow rate 6.7 times greater than that of the more commonly used TSI 3071 model. Humidity is controlled between approximately 20 and 90% through the use of Nafion tube bundles. However, there are variances in the RH during times when the plane was engaged in rapid ascent or descent and the instruments had to adjust to rapid pressure and temperature change. Lastly, the computer was used to regulate the system and record the data.

Analysis of the growth factor distributions collected by this system allows us to characterize the mixing state of the size-resolved aerosol. Cloud droplet concentration for both internally and externally mixed aerosols is dependent upon the peak supersaturation of the cloud. The sensitivity of cloud droplet concentration to aerosol mixing state is dependent upon that supersaturation as well as the aerosol size distribution.

2.4. Optical Thickness and Cloud Albedo

According to Seinfeld and Pandis (1998), the relation between cloud optical thickness and cloud drop number concentration is

$$\tau_c = h\left(\frac{9\pi L^2 N}{2\rho_w^2}\right)^{\frac{1}{3}} \tag{6}$$

where τ_c is the optical thickness of the cloud, h is the actual thickness of the cloud, L is the liquid water content of the cloud, N is the cloud droplet number concentration, and ρ_w is the density of water. This calculated optical thickness is related to cloud albedo through

$$R_c = \frac{\sqrt{3}(1-g)\tau_c}{2+\sqrt{3}(1-g)\tau_c} \tag{7}$$

where R_c is the cloud albedo and g is the so-called asymmetry factor that is the solid angle average of $cos\theta$ weighted by the phase function (Hansen and Pollack, 1970), which is a measure of the degree of forward scattering. Since cloud droplets are much larger than the wavelength of visible light and by assuming a g value of 0.85 (Seinfeld & Pandis, 1998), equation 7 can be simplified to

$$R_c = \frac{\tau_c}{\tau_c + 7.7} \tag{8}$$

The albedo of into which the measured aerosol is introduced can be estimated using these equations. The cloud albedo for internally and externally mixed aerosols are then compared.

3. DATA ANALYSIS

Using software I developed for this project, data charts were created relating particle number concentration (DN/DlogSc) to equally spaced Sc bins (120 bins for scans with 60 counts and 100 bins for scans with 50 counts) for several particle diameters (μm): 0.040, 0.059, 0.086, 0.126, 0.186, 0.273, and 0.400. The initial plots were quite "noisy" and needed to be smoothed in order to establish the general trends within the distributions. Once smoothed, the distributions were categorized as either internally or externally mixed, based upon the number of peaks in the distributions. If a distribution has multiple peaks, then it is categorized as externally mixed, where the peak associated with the lowest Sc results from the most hygroscopic particles of that size and the additional peak(s) correspond to decreasing hygroscopicity. Those distributions containing a single peak were categorized as internally mixed.

3.1. General Observations & Comparisons Across All Scans

A review of the data suggests that while most scans (64 out of the 87 scans analyzed) indicate internal mixtures and contained single peak distributions, a small, not still important, number of distributions possessed multiple peaks. Figure 4 is an example of a distribution reflecting an internally mixed aerosol. It is evident that the distributions shift towards higher Sc with decreasing particle size, as is expected since the solute content of a particle varies with size. At the time the data were collected, there were many natural and anthropogenic aerosol influences, including forest fires, dust storms, and biomass burning to name a few. Figure 5 provides an example of a distribution reflective of an external mixture with multiple peaks in the distributions for particle sizes

0.040 μm, 0.059 μm, and 0.086 μm. The multiple peaks result from particles of the same size originating from two or more different sources. With the exceptions of April 14th Scan #1, April 12th Scan #11, and April 8th Scan #3 (Figures 6 through 8), all of those measurements for which the aerosol was categorized as externally mixed were of particles larger than 0.086 μm. All of the exceptions listed above are for Dp = 0.126 μm. This pronounced size-dependence may be an inherent attribute of the sampled aerosols, where the larger particles have been processed to a greater extent, which results in more uniform composition. Alternatively, the smoothing algorithm may have contributed to the apparent size-dependence by rounding-off the perturbations in the distributions of the larger particles.

In general, the Sc at the peak of the distributions was inversely related to Dp as expected for particles of uniform composition. However, there are a few exceptions (Figures 9 and 15) where larger particles had a higher Sc than some smaller particles. (Note: this was not observed for particles 0.186 μm and larger). This reversal reflects an increase in hygroscopicity with decreasing size, which may result from differing sources of particles within different size modes.

There are also several graphs where the distribution for a particular size seems to dwarf the other distributions. This is demonstrated in Figures 10 and 11, where the distribution for Dp = 0.040 μm peaks at a DN/DlogSc value near 4,200,000 (observed in Figure 10) while the other distributions peak under 12,000 (observed in Figure 11). These distributions could have resulted from the passage of the CIRPAS aircraft through

the exhaust plume left by this, or another, aircraft, or by passing through a ship track where highly concentrated aerosols are found in the atmosphere.

Because dust particles were most concentrated in the free troposphere where overall particle concentrations were lowest, an anticorrelation between predicted CCN concentration and large particle concentration was typically observed. Several scans in this study demonstrate this effect, where large number concentrations of large particles resulted in lowered albedo values. Of the 6 scans where significant distributions of large particles can be observed, 5 were associated with reduced albedo. An example is given in Figure 14 where a significant peak in the 0.400 μm particles is evident. Scans before and after this scan had predicted cumulus cloud albedo in the 0.70's and stratus albedo in the upper 0.20's, while the predicted cloud albedo for the aerosol measured during this scan was 0.69 and 0.21 for cumulus and stratus clouds, respectively. However, there is also one case where high concentrations of large particles are observed with little or no change in albedo between scans (Figure 15). Here, the cumulus and stratus cloud albedo are 0.75 and 0.28 respectively, while the scans before and after also have values in the mid-0.70's and upper 0.20's.

3.2. Daily Observations

Three types of comparisons were made using the distributions and the altitudes at which those distributions were recorded: 1) comparing scans within each atmospheric layer from one scan to the next during each day, 2) comparing the aerosols within given layers measured on different days, and 3) comparing all measurements made throughout

the atmospheric layers for a given day. As stated earlier, three atmospheric layers are identified for these comparisons.

Ranges in Sc for each of the dry sizes (Dp) sampled are given in Tables 20 through 22 for the boundary, pollution, and free troposphere layers respectively. These data show a general decrease in Sc with increasing particle size and an increasing range in Sc with decreasing size.

3.2.1. Comparing Scans Within Each Atmospheric Layer From One Scan to the Next During Each Day

A few general observations can be made by comparing scans from the same atmospheric layer on the same day. The first observation is made when comparing scans within the boundary layer. Observed increases in Sc values coupled with dramatic increases in particle concentrations near the top of the boundary layer indicate the possibility of an elevated pollution layer. This can be observed within the April 19th B scan #'s 1 and 4 (see Figures 18 and 19) with the 0.040 μm particle distributions. This elevated pollution layer appears to dissipate during the day, as afternoon scans exhibit a decrease in 0.040 μm particle concentrations. However, these measurements were made at a lower altitude (<100 meters), which may have been below the elevated pollution layer.

The second observation is that when comparing scans within the pollution layer, as the sampling altitude approaches 1200 meters, both particle concentration and Sc increase. It is also observed that aerosols tend to be externally mixed at that elevation

with internally mixed aerosols above and below. Such an external mixture can be seen in Figure 7 for 0.059 μm in particular.

The third observation is that there were generally lower concentrations in the free troposphere layer. This is expected as wet scavenging of the aerosol depletes the concentration injected into the free troposphere. Although dust concentrations were often highest in the free troposphere, the impact on overall number concentration was relatively small. It is possible that particles smaller than the minimum size measured were present at high concentration in the free troposphere, although these smaller particles would have little impact on cloud microphysics.

3.2.2. Observing Each Layer One Day to the Next Sampled Day

Within the boundary layer, as described earlier, there existed an elevated pollution layer, with 0.040 μm particles being the most concentrated. The more concentrated aerosol sampled in this layer was typically less hygroscopic, which caused a shift towards higher Sc in the inferred distributions. Furthermore, most of the distributions were multimodal, suggesting the aerosol was externally mixed. Above and below this layer, lower particle concentrations and relatively lower Sc values were observed.

The pollution layer was observed to be most concentrated around 1,000 to 1,200 meters in altitude at the beginning of the sampling period. Later in the intensive period, this layer shifted up to 1400+ meters by April 19th, and was no longer observed after April 23rd, as indicated by lowered particles concentrations. The concentrations of 0.04 and 0.059 μm particles were highest in this layer.

3.2.3. Observing/Comparing All Scans Taken and Considered Throughout the Atmospheric Layers for a Given Day

Because the aircraft would often fly close to the boundaries of the different layers observed, it was difficult to quantify spatial variability.

3.3. Cumulus Versus Stratus Cloud Optical Thickness and Albedo

Predicted optical thickness for cumulus clouds was calculated using Equation (6) above, where L = 1.0 g/cm^3, ρ_w = 1.0x10^6 g/cm^3, h = 1,000 m, N = the CCN concentration inferred for that particular scan, and the peak supersaturation was assumed to be 0.5% (Seinfeld & Pandis 1998; Riihimaki 2001). For stratus clouds, it was assumed L = 0.3 g/cm^3, ρ_w = 1.0x10^6 g/cm^3, h = 300 m, and the peak supersaturation was 0.05%. Equation (8) was then used to calculate cloud albedo for both types of clouds. The majority of the scans yielded optical cloud thicknesses under 20 for stratus clouds (94.6%) and > 20 for cumulus clouds (56.5%) with 15 scans yielding values over 100 (see Table 6). The data also have a larger spread across the optical thicknesses for cumulus clouds, ranging from 7 to 328, while that for stratus clouds ranged from 1 to 44.

Cloud albedos were calculated using the optical thickness values calculated previously and Equation (8) above. These values, along with optical cloud thickness and internally mixed/externally mixed classifications, are given in Tables 7 through 17 for each of the days data were collected for this study. The predicted albedos ranged from 48% to 98% for cumulus clouds and 11% to 85% for stratus clouds. When compiled into a frequency chart (Table 18), it is apparent that there is a higher frequency (34.8%) of low stratus albedos (< 0.30) and a higher frequency (69.6%) of high cumulus albedos

(> 0.70). Since cloud albedo is a function of several cloud properties, including thickness and liquid water content, cumulus clouds, which typically have greater vertical extent, are thicker, and have higher liquid water contents, would inherently have higher albedos than stratus clouds.

When the frequency chart is split into internally and externally mixed scans, a couple observations can be made: a) cumulus cloud albedos for both scenarios still have a higher frequency of higher values, and b) stratus cloud albedos for an internally mixed aerosol tend to be low (< 0.3) while those for externally mixed aerosols tend to be higher (between 0.5 and 0.8). This is consistent with the study performed by Hobbs et al. (1980), where they also found that stratus clouds were affected more than cumulus clouds when observing CCN and droplet concentrations in clouds near coal power plants. Their measured increase in cloud droplet concentration would have also increased the cloud albedo.

For this study, scans on April 12th and 14th yielded very high concentrations and accounted for most of the externally mixed samples (Figures 16 and 17). On April 12th, the average optical thicknesses for cumulus and stratus clouds were 93.1 and 12.5. When compared to the average of all the scans in the study, these values were almost 50% higher for both cloud types. However, when comparing cloud albedos, there is a dramatic difference; the increase for cumulus cloud albedo was 13.8%, while that for stratus clouds was 34.0%. For April 14th, similar results were obtained, where cloud optical thicknesses increased by about 60% for both cloud types and stratus cloud albedo

was affected more, with an increase of 45.7% compared to the increase for cumulus clouds of 18.6%.

4. SUMMARY

Using the properties of the aerosol types listed in Table 1, data tables were created relating supersaturations of particles composed of those compounds to relative humidity and growth factor. Aerosol data collected in the vicinity of Japan during ACE-Asia were used in conjunction with these tables to create graphs of differential CCN number concentration versus critical supersaturation. In order to compare one graph to the next, each set of distributions was interpolated onto bins of equally-spaced critical supersaturations and smoothed to reduce noise in the data. The general trends in the distributions were then analyzed and the sampled aerosols were classified as either internally or externally mixed. Lastly, optical depths and albedos of clouds into which the measured aerosol was introduced were calculated for stratus and cumulus clouds to determine any correlations between the mixing states of the aerosols and the resulting cloud albedos.

While the aerosol measured during a majority of the scans was identified as internally mixed, there were enough external mixtures to evaluate the distinction between the two:

a) External mixtures tended to be associated with higher particle concentrations. The higher concentrations were likely a result of pollution from nearby sources and, with a relatively short exposure time to atmospheric mixing, would yield an external mixture.

b) External mixtures were only observed for distributions of particles smaller than 0.186 μm. The larger particles were either pure salts, internal mixtures,

or were external mixtures with very small perturbations in their distributions that the smoothing algorithm smoothed over.

c) Daily observations identified two distinct pollution layers: one elevated within the boundary layer and the other in a frequently observed pollution layer located between 1,000 and 1,400 m above the surface.

d) External mixtures yielded the highest predicted cloud albedo. This relationship is largely the result of an observed increased total concentration associated with external mixtures.

e) Stratus clouds that would form on externally mixed aerosols would be expected to have higher cloud albedos than those associated with internally mixed aerosols, whereas there was little difference in the two for cumulus clouds.

These results are consistent with previous studies; larger aerosol particles yield increased cloud albedos and affect stratus clouds to a greater extent than cumulus clouds.

To further our understanding of the various impacts of mixing state, determining the origins of the aerosols could lead to identification of aerosol migration patterns, dispersion rates, and removal rates in the vicinity of Japan. Using simpler, normalized distributions to identify internally/externally mixed aerosols would result in a more accurate distinction between the two and strengthen the correlations made here.

-

REFERENCES

Ackerman, A. S., O. B. Toon, J. P. Taylor, D. W. Johnson, P. V. Hobbs, and R. J. Ferek, 2000: Effects of aerosols on cloud albedo: Evaluation of Twomey's parameterization of cloud susceptibility using measurements of ship tracks. *J. Atmos. Science*, **57**, 2684-2695.

Brechtel, F. J., and S. M. Kreidenweis, 2000a: Predicting particle critical supersaturation from hydroscopic growth measurements in the humidified TDMA. Part I: Theory and sensitivity studies. *J. Atmos. Sci.*, **57**, 1854-1871.

-----, and S. M. Kreidenweis, 2000b: Predicting particle critical supersaturation from hydroscopic growth measurements in the humidified TDMA. Part II: Laboratory and ambient studies. *J. Atmos. Sci.*, **57**, 1872-1887.

Collins, D. R., H. H. Jonsson, J. H. Seinfeld, R. C. Flagan, S. Gasso, D. A. Hegg, P. B. Russell, B. Schmid, J. M. Livingston, E. Öström, K. J. Noone, L. M. Russell, and J. P. Putaud, 2000: In situ aerosol-size distributions and clear-column radiative closure during ACE-2. *Tellus*, **52B**, 498-525.

Crouzet, Y. and W. H. Marlow, 1995: Calculations of the equilibrium vapor pressure of water over adhering 50-200 nm spheres. *Aerosol Sci. Technol.*, **22**, 43-59.

Facchini, M. C., M. Mircea, S. Fuzzi, and R. J. Charlson, 1999: Cloud albedo enhancement by surface-active organic solutes in growing droplets. *Nature*, **401**, 257-259.

Hansen, J. E. and J. B. Pollack, 1970: Near-infrared light scattering by terrestrial clouds. *J. Atmos. Sci.*, **27**, 265-281.

Hobbs, P. V., T. L. Stith, and L. F. Radke, 1980: Cloud-active nuclei from coal-fired electric power plants and their interactions with clouds. *J. Appl. Meteor.*, **19**, 439-451.

Hudson, J. G., 1991: Observations of anthropogenic cloud condensation nuclei. *Atmos. Envir.*, **25A**, 2449-2455.

Quinn, P. K., T. S. Bates, D. J. Coffman, T. L. Miller, J. E. Johnson, D. S. Covert, J. P. Putaud, C. Neusüb, and T. Novakov, 2000: A comparison of aerosol chemical and optical properties from the 1st and 2nd aerosol characterization experiments, *Tellus*, **52B**, 239-257.

Raymond, T. M., and S. N. Pandis, 2003: Formation of cloud droplets by multicomponent organic particles. *J. Geophys. Res.*, **108 (D15)**, 4469, doi:10.1029/2003JD003503.

Riihimaki, L., 2001: A discussion of cloud albedo and how it could be influenced by (anthropogenic) CCN concentrations. [Available online at http://sciencepolicy.colorado.edu/about_us/archives/projects/gccs/2001/student_work/laura.pdf.]

Seinfeld, J. H. and S. N. Pandis, 1998: *Atmospheric Chemistry and Physics*. John Wiley & Sons, Inc., 75 pp.

Swietlicki, E., J. C. Zhou, D. S. Covert, K. Hameri, B. Busch, M. Vakeva, U. Dusek, O. H. Berg, A. Wiedensohler, P. Aalto, J. Makela, B. G. Martinsson, G. Papaspiropoulos, B. Mentes, G. Frank, and F. Stratmann, 2000: Hygroscopic

properties of aerosol particles in the north-eastern Atlantic during Ace-2. *Tellus*, **52B**, 201-227.

Svenningsson, I. B., H. C. Hansson, A. Wiedensohler, J. A. Ogren, K. J. Noone, and A. Hallberg, 1992: Hydroscopic growth of aerosol particles in the Po Valley. *Tellus*, **44B**, 556-569.

Tang, I. N. and H. R. Munkelwitz, 1994: Water activities, densities, and refractive indices of aqueous sulfates and sodium nitrate droplets of atmospheric importance. *J. Geophys. Res.*, **99,** 18,801-18,808.

-----, 1996: Chemical and size effects of hygroscopic aerosols on light scattering coefficients. *J. Geophys. Res.***, 101**, 19,245-19,250.

-----, A. C. Tridico and K. H. Fung, 1997: Thermodynamic and optical properties of sea salt aerosols. *J. Geophys. Res.*, **102**, 23,296-23,275.

Toon, O., A. Tabazadeh, E. Browell, and J. Jordan, 2000: Analysis of lidar observations of arctic polar stratospheric clouds during January 1989. *J. Geophys. Res*., **105**, 20,589 – 20,615.

Twomey, S., 1991: Aerosols, clouds, and radiation. *Atmos. Envir.*, **25A**, 2435-2442.

Additional Works Consulted

Abdul-Razzak, H., S. J. Ghan, and C. Rivera-Carpio, 1998: A parameterization of aerosol activation. 1. Single aerosol type. *J. Geophys. Res.*, **103 (D6)**, 6123-6131.

-----, and S. J. Ghan, 2000: A parameterization of aerosol activation. 2. Multiple aerosol types. *J. Geophys. Res.*, **105 (D5)**, 6837-6844.

-----, and -----, 2002: A parameterization of aerosol activation. 3. Sectional representation. *J. Geophys. Res.*, **107 (D3)**, 4026, 10.1029/2001JD000483.

-----, and -----, 2004: Parameterization of the influence of organic surfactants on aerosol activation. *J. Geophys. Res.*, **109**, D03205, doi:10.1029/2003JD004043.

Bahreini, R., J. L. Jimenez, J. Wang, R. C. Flagan, J. H. Seinfeld, J. T. Jayne, and D. R. Worsnop, 2003: Aircraft-based aerosol size and composition measurements during ACE-Asia using an Aerodyne aerosol mass spectrometer. *J. Geophys. Res.*, **108 (D23)**, 8645, doi:10.1029/2002JD003226.

Braban, C. F., and J. P. D. Abbatt, 2004: A study of the phase transition behavior of internally mixed ammonium sulfate – malonic acid aerosols. *Atmos. Chem. Phys.*, **4**, 1451-1459.

Buzorius, G., A. Zelenyuk, F. Brechtel, and D. Imre, 2002: Simultaneous determination of individual ambient particle size, hygroscopicity and composition. *Geophys. Res. Lett.*, **29**, NO. 20, 1974, doi:10.1029/2001GL014221.

Cantrell, W., G. Shaw, and R. Benner, 1999: Cloud properties inferred from bimodal aerosol number distributions. *J. Geophys. Res.*, **104 (D22)**, 27,615-27,624.

Clegg, S. L., J. H. Seinfeld, and P. Brimblecombe, 2001: Thermodynamic modeling of aqueous aerosols containing electrolytes and dissolved organic compounds. *J. Aerosol Science*, **32**, 713-738.

Collins, D. R., 2000-2006: Personal Communication, Dept. of Atmospheric Sciences, Texas A & M University.

Huebert, B. J., T. Bates, P. B. Russell, G. Shi, Y. J. Kim, K. Kawamura, G. Carmichael, and T. Nakajima, 2003: An overview of ACE-Asia: Strategies for quantifying the relationships between Asian aerosols and their climatic impacts. *J. Geophys. Res.*, **108 (D23)**, 8633, doi:10.1029/2003JD003550.

Lacis, A. A. and J. E. Hansen, 1974: A parameterization for the absorption of solar radiation in the earth's atmosphere. *J. Atmos. Sci.*, **31**, 118-133.

Saxena, P., L. M. Hildemann, P. H. McMurry, and J. H. Seinfeld, 1995: Organics alter hygroscopic behavior of atmospheric particles. *J. Geophys. Res.*, **100 (D9)**, 18,755-18,770.

Tegen, I. and A. A. Lacis, 1996: Modeling of particle size distribution and its influence on the radiative properties of mineral dust aerosol. *J. Geophys. Res*., **101** (**D14)**, 19,237-19,244.

Xie, J. and W. H. Marlow, 1997: Water vapor pressure over complex particles, I: sulfuric acid solution effect. *Aerosol Sci. Technol.*, **27**, 591-603.

Zhang, X. Q., P. H. McMurry, S. V. Hering, and G. S. Casuccio, 1993: Mixing characteristics and water content of submicron aerosols measured in Los Angeles and at the Grand Canyon. *Atmos. Environ*., **27A**, 1593-1607.

APPENDIX A

TABLES

Table 1. Shown here are the polynomial coefficients for water activities and densities that were used in the Köhler Equation for the compounds/species considered. (From Tang and Munkelwitz, 1994; Tang, 1996; Tang et al., 1997)

	$(NH_4)_2SO_4$	NH_4HSO_4	NaCl	H_2SO_4	NH_4NO_3
x_1 %	0-78	0-97	0-45	---	---
C_1	-2.715 (-3)*	-3.050 (-3)	-6.366 (-3)	-5.196 (-3)	-3.650 (-3)
C_2	3.113 (-5)	-2.940 (-5)	8.624 (-5)	9.746 (-5)	-9.155 (-6)
C_3	-2.336 (-6)	-4.430 (-7)	-1.158 (-5)	-9.693 (-6)	-2.826 (-7)
C_4	1.412 (-8)	---	1.518 (-7)	9.405 (-8)	0
A_1	5.920 (-3)	5.870 (-3)	7.410 (-3)	7.367 (-3)	4.050 (-3)
A_2	-5.036 (-6)	-1.890 (-6)	-3.741 (-5)	-4.934 (-5)	9.000 (-6)
A_3	1.024 (-8)	1.763 (-7)	2.252 (-6)	1.754 (-6)	0
A_4	---	---	-2.060 (-8)	-1.104 (-8)	0
Density	1.76	1.78	2.165	1.83	1.725

* Read -2.715×10^{-3}

Table 2. This table is an example of the charts used by the program RunFirst.f. It contains all the possible minimum critical supersaturation values for the salts considered in Table 1 given relative humidity and growth factor for particles of size Dp = 0.040μm.

Minimum Critical Supersaturations: Dp = 0.040

(corresponding to a given growth factor and relative humidity)

Relative Humidity (%)

Growth Factor (%)	80	81	82	83	84	85	86	87	88	89	90	91	92	93	94	95	96
1.00	0.0055	0.0055	0.0055	0.0055	0.0055	0.0055	0.0055	0.0055	0.0055	0.0055	0.0055	0.0055	0.0055	0.0055	0.0055	0.0055	0.0055
1.03	0.0055	0.0076	0.0132	0.0136	0.0141	0.0146	0.0151	0.0155	0.0159	0.0166	0.0171	0.0177	0.0183	0.0189	0.0196	0.0203	0.0211
1.06	0.0055	0.0076	0.0103	0.0106	0.0110	0.0114	0.0118	0.0122	0.0126	0.0130	0.0134	0.0139	0.0144	0.0149	0.0154	0.0160	0.0167
1.09	0.0055	0.0076	0.0088	0.0092	0.0095	0.0098	0.0101	0.0105	0.0108	0.0112	0.0116	0.0120	0.0124	0.0129	0.0134	0.0139	0.0144
1.12	0.0055	0.0076	0.0079	0.0082	0.0085	0.0088	0.0091	0.0094	0.0097	0.0101	0.0104	0.0108	0.0112	0.0116	0.0120	0.0125	0.0130
1.15	0.0055	0.0076	0.0073	0.0075	0.0078	0.0081	0.0083	0.0086	0.0089	0.0093	0.0096	0.0099	0.0103	0.0107	0.0111	0.0115	0.0120
1.18	0.0055	0.0076	0.0067	0.0070	0.0072	0.0075	0.0078	0.0080	0.0083	0.0086	0.0089	0.0092	0.0096	0.0099	0.0103	0.0107	0.0112
1.21	0.0055	0.0076	0.0059	0.0066	0.0068	0.0070	0.0073	0.0076	0.0078	0.0081	0.0084	0.0087	0.0090	0.0094	0.0097	0.0101	0.0106
1.24	0.0055	0.0076	0.0060	0.0062	0.0064	0.0067	0.0069	0.0071	0.0074	0.0077	0.0079	0.0082	0.0085	0.0089	0.0092	0.0096	0.0100
1.27	0.0055	0.0055	0.0057	0.0059	0.0061	0.0063	0.0066	0.0068	0.0070	0.0073	0.0076	0.0078	0.0081	0.0084	0.0088	0.0091	0.0096
1.30	0.0055	0.0052	0.0054	0.0056	0.0058	0.0061	0.0063	0.0065	0.0067	0.0070	0.0072	0.0075	0.0078	0.0081	0.0084	0.0088	0.0092
1.33	0.0055	0.0050	0.0052	0.0054	0.0056	0.0058	0.0060	0.0062	0.0065	0.0067	0.0069	0.0072	0.0075	0.0078	0.0081	0.0084	0.0088
1.36	0.0055	0.0048	0.0050	0.0052	0.0054	0.0056	0.0058	0.0060	0.0062	0.0064	0.0067	0.0069	0.0072	0.0075	0.0078	0.0081	0.0085
1.39	0.0055	0.0046	0.0048	0.0050	0.0052	0.0054	0.0056	0.0058	0.0060	0.0062	0.0064	0.0067	0.0069	0.0072	0.0075	0.0078	0.0082
1.42	0.0055	0.0045	0.0046	0.0048	0.0050	0.0052	0.0054	0.0056	0.0058	0.0060	0.0062	0.0065	0.0067	0.0070	0.0073	0.0076	0.0079
1.45	0.0055	0.0043	0.0045	0.0047	0.0048	0.0050	0.0052	0.0054	0.0056	0.0058	0.0060	0.0062	0.0065	0.0068	0.0070	0.0073	0.0077
1.48	0.0055	0.0042	0.0044	0.0045	0.0047	0.0049	0.0050	0.0052	0.0054	0.0056	0.0058	0.0061	0.0063	0.0065	0.0068	0.0071	0.0075
1.51	0.0055	0.0041	0.0042	0.0044	0.0045	0.0047	0.0049	0.0051	0.0053	0.0055	0.0057	0.0059	0.0061	0.0064	0.0066	0.0069	0.0073
1.54	0.0055	0.0039	0.0041	0.0043	0.0044	0.0046	0.0048	0.0049	0.0051	0.0053	0.0055	0.0057	0.0059	0.0062	0.0065	0.0068	0.0071
1.57	0.0055	0.0038	0.0040	0.0041	0.0043	0.0045	0.0046	0.0048	0.0050	0.0052	0.0054	0.0056	0.0058	0.0060	0.0063	0.0066	0.0069
1.60	0.0055	0.0037	0.0039	0.0040	0.0042	0.0043	0.0045	0.0047	0.0048	0.0050	0.0052	0.0054	0.0056	0.0059	0.0061	0.0064	0.0067
1.63	0.0055	0.0036	0.0038	0.0039	0.0041	0.0042	0.0044	0.0046	0.0047	0.0049	0.0051	0.0053	0.0055	0.0057	0.0060	0.0063	0.0066
1.66	0.0055	0.0057	0.0037	0.0038	0.0040	0.0041	0.0043	0.0044	0.0046	0.0048	0.0050	0.0052	0.0054	0.0056	0.0058	0.0061	0.0064
1.69	0.0054	0.0055	0.0036	0.0037	0.0039	0.0040	0.0042	0.0043	0.0045	0.0047	0.0049	0.0050	0.0052	0.0055	0.0057	0.0060	0.0063
1.72	0.0052	0.0053	0.0054	0.0036	0.0038	0.0039	0.0041	0.0042	0.0044	0.0046	0.0047	0.0049	0.0051	0.0053	0.0056	0.0059	0.0062
1.75	0.0051	0.0051	0.0052	0.0036	0.0037	0.0038	0.0040	0.0041	0.0043	0.0045	0.0046	0.0048	0.0050	0.0052	0.0055	0.0057	0.0060
1.78	0.0000	0.0000	0.0051	0.0052	0.0036	0.0038	0.0039	0.0040	0.0042	0.0044	0.0045	0.0047	0.0049	0.0051	0.0054	0.0056	0.0059
1.81	0.0000	0.0000	0.0000	0.0050	0.0051	0.0037	0.0038	0.0040	0.0041	0.0043	0.0044	0.0046	0.0048	0.0050	0.0052	0.0055	0.0058
1.84	0.0000	0.0000	0.0000	0.0000	0.0000	0.0036	0.0037	0.0039	0.0040	0.0042	0.0043	0.0045	0.0047	0.0049	0.0051	0.0054	0.0057
1.87	0.0000	0.0000	0.0000	0.0000	0.0000	0.0000	0.0037	0.0038	0.0039	0.0041	0.0043	0.0044	0.0046	0.0048	0.0050	0.0053	0.0056
1.90	0.0000	0.0000	0.0000	0.0000	0.0000	0.0000	0.0036	0.0037	0.0039	0.0040	0.0042	0.0043	0.0045	0.0047	0.0049	0.0052	0.0055
1.93	0.0000	0.0000	0.0000	0.0000	0.0000	0.0000	0.0000	0.0036	0.0038	0.0039	0.0041	0.0043	0.0044	0.0046	0.0049	0.0051	0.0054
1.96	0.0000	0.0000	0.0000	0.0000	0.0000	0.0000	0.0000	0.0036	0.0037	0.0039	0.0040	0.0042	0.0044	0.0046	0.0048	0.0050	0.0053
1.99	0.0000	0.0000	0.0000	0.0000	0.0000	0.0000	0.0000	0.0000	0.0036	0.0038	0.0039	0.0041	0.0043	0.0045	0.0047	0.0049	0.0052
2.02	0.0000	0.0000	0.0000	0.0000	0.0000	0.0000	0.0000	0.0000	0.0036	0.0037	0.0039	0.0040	0.0042	0.0044	0.0046	0.0048	0.0051
2.05	0.0000	0.0000	0.0000	0.0000	0.0000	0.0000	0.0000	0.0000	0.0000	0.0037	0.0038	0.0040	0.0041	0.0043	0.0045	0.0048	0.0050
2.08	0.0000	0.0000	0.0000	0.0000	0.0000	0.0000	0.0000	0.0000	0.0000	0.0036	0.0037	0.0039	0.0041	0.0042	0.0044	0.0047	0.0049
2.11	0.0000	0.0000	0.0000	0.0000	0.0000	0.0000	0.0000	0.0000	0.0000	0.0000	0.0037	0.0038	0.0040	0.0042	0.0044	0.0046	0.0049
2.14	0.0000	0.0000	0.0000	0.0000	0.0000	0.0000	0.0000	0.0000	0.0000	0.0000	0.0036	0.0038	0.0039	0.0041	0.0043	0.0045	0.0048
2.17	0.0000	0.0000	0.0000	0.0000	0.0000	0.0000	0.0000	0.0000	0.0000	0.0000	0.0000	0.0037	0.0039	0.0040	0.0042	0.0045	0.0047
2.20	0.0000	0.0000	0.0000	0.0000	0.0000	0.0000	0.0000	0.0000	0.0000	0.0000	0.0000	0.0036	0.0038	0.0040	0.0042	0.0044	0.0046
2.23	0.0000	0.0000	0.0000	0.0000	0.0000	0.0000	0.0000	0.0000	0.0000	0.0000	0.0000	0.0036	0.0037	0.0039	0.0041	0.0043	0.0046
2.26	0.0000	0.0000	0.0000	0.0000	0.0000	0.0000	0.0000	0.0000	0.0000	0.0000	0.0000	0.0000	0.0037	0.0038	0.0040	0.0043	0.0045
2.29	0.0000	0.0000	0.0000	0.0000	0.0000	0.0000	0.0000	0.0000	0.0000	0.0000	0.0000	0.0000	0.0036	0.0038	0.0040	0.0042	0.0044
2.32	0.0000	0.0000	0.0000	0.0000	0.0000	0.0000	0.0000	0.0000	0.0000	0.0000	0.0000	0.0000	0.0036	0.0037	0.0039	0.0041	0.0044
2.35	0.0000	0.0000	0.0000	0.0000	0.0000	0.0000	0.0000	0.0000	0.0000	0.0000	0.0000	0.0000	0.0000	0.0037	0.0039	0.0041	0.0043
2.38	0.0000	0.0000	0.0000	0.0000	0.0000	0.0000	0.0000	0.0000	0.0000	0.0000	0.0000	0.0000	0.0000	0.0036	0.0038	0.0040	0.0043
2.41	0.0000	0.0000	0.0000	0.0000	0.0000	0.0000	0.0000	0.0000	0.0000	0.0000	0.0000	0.0000	0.0000	0.0036	0.0037	0.0040	0.0042
2.44	0.0000	0.0000	0.0000	0.0000	0.0000	0.0000	0.0000	0.0000	0.0000	0.0000	0.0000	0.0000	0.0000	0.0000	0.0037	0.0039	0.0041
2.47	0.0000	0.0000	0.0000	0.0000	0.0000	0.0000	0.0000	0.0000	0.0000	0.0000	0.0000	0.0000	0.0000	0.0000	0.0036	0.0038	0.0041
2.50	0.0000	0.0000	0.0000	0.0000	0.0000	0.0000	0.0000	0.0000	0.0000	0.0000	0.0000	0.0000	0.0000	0.0000	0.0036	0.0038	0.0040

Table 3. This table is an example of the charts used by the program RunFirst.f. It contains all the possible maximum critical supersaturation values for the salts considered in Table 1 given relative humidity and growth factor for particles of size Dp = 0.040μm.

Maximum Critical Supersaturations: Dp = 0.040

(corresponding to a given growth factor and relative humidity)

Growth Factor (%) \ Relative Humidity (%)	80	81	82	83	84	85	86	87	88	89	90	91	92	93	94	95	96
1.00	0.0117	0.0117	0.0117	0.0117	0.0117	0.0117	0.0117	0.0117	0.0117	0.0117	0.0117	0.0117	0.0117	0.0117	0.0117	0.0117	0.0117
1.03	0.0280	0.0283	0.0283	0.0289	0.0292	0.0295	0.0299	0.0302	0.0306	0.0310	0.0315	0.0319	0.0324	0.0329	0.0336	0.0343	0.0352
1.06	0.0217	0.0220	0.0223	0.0225	0.0229	0.0233	0.0236	0.0240	0.0244	0.0248	0.0253	0.0257	0.0263	0.0268	0.0276	0.0284	0.0293
1.09	0.0182	0.0185	0.0187	0.0190	0.0193	0.0193	0.0198	0.0203	0.0207	0.0211	0.0216	0.0220	0.0226	0.0231	0.0239	0.0247	0.0257
1.12	0.0158	0.0161	0.0163	0.0166	0.0169	0.0172	0.0175	0.0178	0.0182	0.0186	0.0190	0.0195	0.0200	0.0206	0.0213	0.0221	0.0231
1.15	0.0141	0.0143	0.0146	0.0148	0.0151	0.0154	0.0157	0.0160	0.0163	0.0167	0.0171	0.0175	0.0180	0.0186	0.0193	0.0202	0.0211
1.18	0.0128	0.0130	0.0132	0.0135	0.0137	0.0140	0.0142	0.0145	0.0149	0.0152	0.0156	0.0160	0.0164	0.0171	0.0178	0.0185	0.0194
1.21	0.0117	0.0119	0.0122	0.0124	0.0126	0.0128	0.0131	0.0134	0.0137	0.0140	0.0144	0.0148	0.0152	0.0158	0.0165	0.0172	0.0181
1.24	0.0109	0.0111	0.0112	0.0114	0.0117	0.0119	0.0121	0.0124	0.0127	0.0130	0.0133	0.0137	0.0142	0.0147	0.0154	0.0161	0.0170
1.27	0.0101	0.0103	0.0105	0.0107	0.0109	0.0111	0.0113	0.0116	0.0116	0.0122	0.0125	0.0128	0.0133	0.0138	0.0145	0.0152	0.0160
1.30	0.0095	0.0097	0.0098	0.0100	0.0102	0.0104	0.0106	0.0109	0.0111	0.0114	0.0117	0.0121	0.0125	0.0131	0.0137	0.0143	0.0151
1.33	0.0090	0.0091	0.0093	0.0094	0.0096	0.0098	0.0100	0.0103	0.0105	0.0108	0.0111	0.0114	0.0119	0.0124	0.0129	0.0136	0.0144
1.36	0.0085	0.0086	0.0088	0.0089	0.0091	0.0093	0.0095	0.0097	0.0100	0.0102	0.0105	0.0108	0.0113	0.0118	0.0123	0.0130	0.0137
1.39	0.0080	0.0082	0.0083	0.0085	0.0087	0.0088	0.0090	0.0092	0.0095	0.0097	0.0100	0.0103	0.0107	0.0112	0.0118	0.0124	0.0131
1.42	0.0077	0.0078	0.0079	0.0081	0.0083	0.0084	0.0086	0.0088	0.0090	0.0093	0.0095	0.0099	0.0102	0.0107	0.0112	0.0118	0.0126
1.45	0.0073	0.0074	0.0076	0.0077	0.0079	0.0080	0.0082	0.0082	0.0086	0.0089	0.0091	0.0094	0.0098	0.0103	0.0108	0.0114	0.0121
1.48	0.0070	0.0071	0.0073	0.0074	0.0075	0.0077	0.0079	0.0081	0.0083	0.0085	0.0087	0.0091	0.0094	0.0099	0.0104	0.0109	0.0116
1.51	0.0067	0.0068	0.0070	0.0071	0.0072	0.0074	0.0076	0.0077	0.0079	0.0081	0.0084	0.0087	0.0091	0.0095	0.0100	0.0105	0.0112
1.54	0.0064	0.0066	0.0067	0.0068	0.0070	0.0071	0.0073	0.0074	0.0076	0.0078	0.0081	0.0084	0.0087	0.0091	0.0096	0.0102	0.0108
1.57	0.0062	0.0063	0.0064	0.0066	0.0067	0.0068	0.0070	0.0072	0.0073	0.0075	0.0078	0.0081	0.0084	0.0088	0.0093	0.0098	0.0104
1.60	0.0060	0.0061	0.0062	0.0063	0.0064	0.0066	0.0067	0.0069	0.0071	0.0073	0.0075	0.0078	0.0081	0.0085	0.0090	0.0095	0.0101
1.63	0.0058	0.0059	0.0060	0.0061	0.0062	0.0064	0.0065	0.0067	0.0068	0.0070	0.0072	0.0075	0.0079	0.0082	0.0087	0.0092	0.0098
1.66	0.0056	0.0057	0.0058	0.0059	0.0060	0.0061	0.0063	0.0064	0.0066	0.0068	0.0070	0.0073	0.0076	0.0080	0.0084	0.0089	0.0095
1.69	0.0055	0.0055	0.0056	0.0057	0.0058	0.0059	0.0061	0.0062	0.0064	0.0066	0.0068	0.0071	0.0074	0.0077	0.0082	0.0086	0.0092
1.72	0.0000	0.0053	0.0054	0.0055	0.0056	0.0058	0.0059	0.0060	0.0062	0.0064	0.0066	0.0069	0.0072	0.0075	0.0079	0.0084	0.0089
1.75	0.0000	0.0051	0.0052	0.0053	0.0055	0.0056	0.0057	0.0058	0.0060	0.0062	0.0064	0.0067	0.0070	0.0073	0.0077	0.0081	0.0087
1.78	0.0000	0.0000	0.0051	0.0052	0.0053	0.0054	0.0055	0.0057	0.0058	0.0060	0.0062	0.0064	0.0068	0.0071	0.0075	0.0079	0.0085
1.81	0.0000	0.0000	0.0000	0.0050	0.0051	0.0053	0.0054	0.0055	0.0057	0.0058	0.0060	0.0062	0.0066	0.0069	0.0073	0.0077	0.0082
1.84	0.0000	0.0000	0.0000	0.0000	0.0000	0.0051	0.0052	0.0054	0.0055	0.0057	0.0058	0.0060	0.0063	0.0067	0.0071	0.0075	0.0080
1.87	0.0000	0.0000	0.0000	0.0000	0.0000	0.0000	0.0051	0.0052	0.0053	0.0055	0.0057	0.0059	0.0061	0.0063	0.0069	0.0073	0.0078
1.90	0.0000	0.0000	0.0000	0.0000	0.0000	0.0000	0.0036	0.0051	0.0052	0.0054	0.0055	0.0057	0.0059	0.0062	0.0067	0.0071	0.0076
1.93	0.0000	0.0000	0.0000	0.0000	0.0000	0.0000	0.0000	0.0036	0.0051	0.0052	0.0054	0.0056	0.0058	0.0060	0.0063	0.0070	0.0075
1.96	0.0000	0.0000	0.0000	0.0000	0.0000	0.0000	0.0000	0.0036	0.0037	0.0051	0.0052	0.0054	0.0056	0.0059	0.0062	0.0068	0.0073
1.99	0.0000	0.0000	0.0000	0.0000	0.0000	0.0000	0.0000	0.0000	0.0036	0.0038	0.0051	0.0053	0.0055	0.0057	0.0060	0.0066	0.0071
2.02	0.0000	0.0000	0.0000	0.0000	0.0000	0.0000	0.0000	0.0000	0.0036	0.0037	0.0039	0.0052	0.0054	0.0056	0.0059	0.0062	0.0070
2.05	0.0000	0.0000	0.0000	0.0000	0.0000	0.0000	0.0000	0.0000	0.0000	0.0037	0.0038	0.0050	0.0052	0.0055	0.0057	0.0061	0.0068
2.08	0.0000	0.0000	0.0000	0.0000	0.0000	0.0000	0.0000	0.0000	0.0000	0.0036	0.0037	0.0039	0.0051	0.0053	0.0056	0.0059	0.0067
2.11	0.0000	0.0000	0.0000	0.0000	0.0000	0.0000	0.0000	0.0000	0.0000	0.0000	0.0037	0.0038	0.0050	0.0053	0.0055	0.0058	0.0062
2.14	0.0000	0.0000	0.0000	0.0000	0.0000	0.0000	0.0000	0.0000	0.0000	0.0000	0.0036	0.0038	0.0039	0.0051	0.0054	0.0057	0.0061
2.17	0.0000	0.0000	0.0000	0.0000	0.0000	0.0000	0.0000	0.0000	0.0000	0.0000	0.0000	0.0037	0.0039	0.0040	0.0052	0.0056	0.0059
2.20	0.0000	0.0000	0.0000	0.0000	0.0000	0.0000	0.0000	0.0000	0.0000	0.0000	0.0000	0.0036	0.0038	0.0040	0.0051	0.0054	0.0058
2.23	0.0000	0.0000	0.0000	0.0000	0.0000	0.0000	0.0000	0.0000	0.0000	0.0000	0.0000	0.0036	0.0037	0.0039	0.0050	0.0053	0.0057
2.26	0.0000	0.0000	0.0000	0.0000	0.0000	0.0000	0.0000	0.0000	0.0000	0.0000	0.0000	0.0000	0.0037	0.0038	0.0040	0.0052	0.0056
2.29	0.0000	0.0000	0.0000	0.0000	0.0000	0.0000	0.0000	0.0000	0.0000	0.0000	0.0000	0.0000	0.0036	0.0038	0.0040	0.0051	0.0055
2.32	0.0000	0.0000	0.0000	0.0000	0.0000	0.0000	0.0000	0.0000	0.0000	0.0000	0.0000	0.0000	0.0036	0.0037	0.0039	0.0050	0.0054
2.35	0.0000	0.0000	0.0000	0.0000	0.0000	0.0000	0.0000	0.0000	0.0000	0.0000	0.0000	0.0000	0.0000	0.0037	0.0039	0.0041	0.0053
2.38	0.0000	0.0000	0.0000	0.0000	0.0000	0.0000	0.0000	0.0000	0.0000	0.0000	0.0000	0.0000	0.0000	0.0036	0.0038	0.0040	0.0052
2.41	0.0000	0.0000	0.0000	0.0000	0.0000	0.0000	0.0000	0.0000	0.0000	0.0000	0.0000	0.0000	0.0000	0.0036	0.0037	0.0040	0.0051
2.44	0.0000	0.0000	0.0000	0.0000	0.0000	0.0000	0.0000	0.0000	0.0000	0.0000	0.0000	0.0000	0.0000	0.0000	0.0037	0.0039	0.0041
2.47	0.0000	0.0000	0.0000	0.0000	0.0000	0.0000	0.0000	0.0000	0.0000	0.0000	0.0000	0.0000	0.0000	0.0000	0.0036	0.0038	0.0041
2.50	0.0000	0.0000	0.0000	0.0000	0.0000	0.0000	0.0000	0.0000	0.0000	0.0000	0.0000	0.0000	0.0000	0.0000	0.0036	0.0038	0.0040

Table 4. This table is an example of the charts used by the program RunFirst.f. It contains all the possible average critical supersaturation values for the salts considered in Table 1 given relative humidity and growth factor for particles of size Dp = 0.040μm.

Average Critical Supersaturations: Dp = 0.040

(corresponding to a given growth factor and relative humidity)

Growth Factor (%) \ Relative Humidity	80%	81%	82%	83%	84%	85%	86%	87%	88%	89%	90%	91%	92%	93%	94%	95%	96%
1.00	0.0093	0.0093	0.0093	0.0093	0.0093	0.0093	0.0093	0.0093	0.0093	0.0093	0.0093	0.0093	0.0093	0.0093	0.0093	0.0093	0.0093
1.03	0.0219	0.0226	0.0240	0.0245	0.0249	0.0253	0.0258	0.0262	0.0267	0.0272	0.0278	0.0283	0.0289	0.0296	0.0303	0.0310	0.0318
1.06	0.0171	0.0178	0.0186	0.0190	0.0194	0.0198	0.0202	0.0206	0.0211	0.0216	0.0221	0.0226	0.0232	0.0239	0.0245	0.0253	0.0261
1.09	0.0145	0.0151	0.0157	0.0160	0.0163	0.0166	0.0171	0.0175	0.0180	0.0184	0.0189	0.0194	0.0200	0.0206	0.0212	0.0220	0.0228
1.12	0.0128	0.0134	0.0137	0.0140	0.0143	0.0147	0.0150	0.0154	0.0158	0.0162	0.0167	0.0172	0.0177	0.0183	0.0189	0.0196	0.0204
1.15	0.0115	0.0121	0.0123	0.0126	0.0128	0.0132	0.0135	0.0139	0.0142	0.0147	0.0151	0.0155	0.0160	0.0166	0.0172	0.0179	0.0187
1.18	0.0105	0.0111	0.0112	0.0114	0.0117	0.0120	0.0123	0.0127	0.0130	0.0134	0.0138	0.0142	0.0147	0.0153	0.0159	0.0165	0.0173
1.21	0.0098	0.0103	0.0102	0.0105	0.0108	0.0111	0.0114	0.0117	0.0120	0.0124	0.0128	0.0132	0.0136	0.0142	0.0147	0.0154	0.0161
1.24	0.0091	0.0097	0.0096	0.0098	0.0101	0.0103	0.0106	0.0109	0.0112	0.0116	0.0119	0.0123	0.0128	0.0133	0.0138	0.0144	0.0151
1.27	0.0086	0.0087	0.0089	0.0092	0.0094	0.0097	0.0099	0.0102	0.0104	0.0108	0.0112	0.0116	0.0120	0.0125	0.0130	0.0136	0.0143
1.30	0.0081	0.0082	0.0084	0.0086	0.0089	0.0091	0.0094	0.0096	0.0099	0.0102	0.0106	0.0109	0.0113	0.0118	0.0123	0.0129	0.0135
1.33	0.0077	0.0078	0.0080	0.0082	0.0084	0.0086	0.0088	0.0091	0.0094	0.0097	0.0100	0.0104	0.0107	0.0112	0.0117	0.0122	0.0129
1.36	0.0074	0.0074	0.0075	0.0077	0.0079	0.0082	0.0084	0.0086	0.0089	0.0092	0.0095	0.0098	0.0102	0.0106	0.0111	0.0117	0.0123
1.39	0.0070	0.0070	0.0072	0.0074	0.0076	0.0078	0.0080	0.0082	0.0085	0.0088	0.0091	0.0094	0.0098	0.0102	0.0106	0.0112	0.0118
1.42	0.0068	0.0067	0.0069	0.0070	0.0072	0.0074	0.0076	0.0079	0.0081	0.0084	0.0087	0.0090	0.0093	0.0097	0.0102	0.0107	0.0113
1.45	0.0065	0.0064	0.0066	0.0067	0.0069	0.0071	0.0073	0.0071	0.0078	0.0080	0.0083	0.0086	0.0090	0.0093	0.0098	0.0103	0.0109
1.48	0.0063	0.0060	0.0061	0.0065	0.0066	0.0068	0.0070	0.0072	0.0074	0.0077	0.0080	0.0083	0.0086	0.0090	0.0094	0.0099	0.0105
1.51	0.0061	0.0054	0.0056	0.0061	0.0062	0.0065	0.0067	0.0069	0.0072	0.0074	0.0077	0.0080	0.0083	0.0086	0.0091	0.0095	0.0101
1.54	0.0060	0.0053	0.0054	0.0055	0.0060	0.0062	0.0063	0.0067	0.0069	0.0071	0.0074	0.0077	0.0080	0.0083	0.0087	0.0092	0.0098
1.57	0.0059	0.0051	0.0052	0.0053	0.0055	0.0060	0.0061	0.0063	0.0067	0.0069	0.0071	0.0074	0.0077	0.0080	0.0084	0.0089	0.0094
1.60	0.0057	0.0049	0.0050	0.0052	0.0053	0.0055	0.0056	0.0061	0.0063	0.0067	0.0069	0.0072	0.0074	0.0078	0.0082	0.0086	0.0091
1.63	0.0056	0.0048	0.0049	0.0050	0.0051	0.0053	0.0054	0.0056	0.0061	0.0063	0.0067	0.0069	0.0072	0.0075	0.0079	0.0083	0.0089
1.66	0.0055	0.0057	0.0047	0.0049	0.0050	0.0051	0.0053	0.0054	0.0056	0.0061	0.0064	0.0067	0.0070	0.0073	0.0077	0.0081	0.0086
1.69	0.0055	0.0055	0.0046	0.0047	0.0048	0.0050	0.0051	0.0053	0.0054	0.0056	0.0062	0.0064	0.0068	0.0071	0.0074	0.0079	0.0084
1.72	0.0054	0.0053	0.0054	0.0046	0.0047	0.0048	0.0050	0.0051	0.0053	0.0055	0.0060	0.0062	0.0065	0.0069	0.0072	0.0076	0.0081
1.75	0.0053	0.0051	0.0052	0.0045	0.0046	0.0047	0.0048	0.0050	0.0051	0.0053	0.0055	0.0061	0.0063	0.0066	0.0070	0.0074	0.0079
1.78	0.0052	0.0050	0.0051	0.0043	0.0045	0.0046	0.0047	0.0049	0.0050	0.0052	0.0054	0.0056	0.0061	0.0064	0.0068	0.0072	0.0077
1.81	0.0051	0.0048	0.0049	0.0042	0.0043	0.0045	0.0046	0.0047	0.0049	0.0050	0.0052	0.0054	0.0059	0.0063	0.0066	0.0070	0.0075
1.84	0.0050	0.0047	0.0048	0.0041	0.0042	0.0043	0.0045	0.0046	0.0048	0.0049	0.0051	0.0053	0.0055	0.0061	0.0064	0.0069	0.0073
1.87	0.0050	0.0045	0.0046	0.0039	0.0041	0.0042	0.0044	0.0045	0.0046	0.0048	0.0050	0.0052	0.0054	0.0058	0.0063	0.0066	0.0071
1.90	0.0049	0.0043	0.0045	0.0038	0.0040	0.0041	0.0043	0.0044	0.0045	0.0047	0.0049	0.0050	0.0052	0.0055	0.0061	0.0065	0.0070
1.93	0.0048	0.0042	0.0043	0.0037	0.0038	0.0040	0.0041	0.0043	0.0044	0.0046	0.0047	0.0049	0.0051	0.0053	0.0058	0.0063	0.0068
1.96	0.0047	0.0040	0.0041	0.0036	0.0037	0.0039	0.0040	0.0042	0.0043	0.0045	0.0046	0.0048	0.0050	0.0052	0.0055	0.0062	0.0066
1.99	0.0046	0.0038	0.0040	0.0034	0.0036	0.0038	0.0039	0.0041	0.0042	0.0044	0.0045	0.0047	0.0049	0.0051	0.0053	0.0059	0.0065
2.02	0.0046	0.0037	0.0038	0.0033	0.0035	0.0037	0.0038	0.0040	0.0041	0.0043	0.0044	0.0046	0.0048	0.0050	0.0052	0.0057	0.0063
2.05	0.0045	0.0035	0.0037	0.0032	0.0033	0.0036	0.0037	0.0039	0.0040	0.0042	0.0043	0.0045	0.0047	0.0049	0.0051	0.0054	0.0062
2.08	0.0044	0.0033	0.0035	0.0030	0.0032	0.0034	0.0036	0.0037	0.0039	0.0041	0.0042	0.0044	0.0046	0.0048	0.0050	0.0053	0.0061
2.11	0.0043	0.0032	0.0033	0.0029	0.0031	0.0033	0.0035	0.0036	0.0038	0.0040	0.0041	0.0043	0.0045	0.0047	0.0049	0.0052	0.0058
2.14	0.0042	0.0030	0.0032	0.0028	0.0030	0.0032	0.0034	0.0035	0.0037	0.0039	0.0040	0.0042	0.0044	0.0046	0.0048	0.0051	0.0054
2.17	0.0042	0.0029	0.0030	0.0027	0.0029	0.0031	0.0032	0.0034	0.0036	0.0037	0.0039	0.0041	0.0043	0.0046	0.0047	0.0050	0.0053
2.20	0.0041	0.0027	0.0029	0.0025	0.0027	0.0030	0.0031	0.0033	0.0035	0.0036	0.0038	0.0040	0.0042	0.0045	0.0047	0.0049	0.0052
2.23	0.0040	0.0025	0.0027	0.0024	0.0026	0.0029	0.0030	0.0032	0.0034	0.0035	0.0037	0.0039	0.0041	0.0044	0.0046	0.0048	0.0051
2.26	0.0039	0.0024	0.0026	0.0023	0.0025	0.0028	0.0029	0.0031	0.0033	0.0034	0.0036	0.0038	0.0040	0.0043	0.0045	0.0047	0.0050
2.29	0.0038	0.0022	0.0024	0.0021	0.0024	0.0027	0.0028	0.0030	0.0032	0.0033	0.0035	0.0037	0.0039	0.0043	0.0044	0.0047	0.0050
2.32	0.0037	0.0020	0.0022	0.0020	0.0022	0.0025	0.0027	0.0029	0.0031	0.0032	0.0034	0.0036	0.0039	0.0042	0.0043	0.0046	0.0049
2.35	0.0037	0.0019	0.0021	0.0019	0.0021	0.0024	0.0026	0.0028	0.0029	0.0031	0.0033	0.0035	0.0038	0.0041	0.0042	0.0045	0.0048
2.38	0.0036	0.0017	0.0019	0.0018	0.0020	0.0023	0.0025	0.0027	0.0028	0.0030	0.0032	0.0034	0.0037	0.0040	0.0041	0.0044	0.0047
2.41	0.0035	0.0015	0.0018	0.0016	0.0019	0.0022	0.0024	0.0026	0.0027	0.0029	0.0031	0.0033	0.0036	0.0039	0.0041	0.0043	0.0046
2.44	0.0034	0.0014	0.0016	0.0015	0.0017	0.0021	0.0022	0.0024	0.0026	0.0028	0.0030	0.0032	0.0035	0.0039	0.0040	0.0043	0.0046
2.47	0.0033	0.0012	0.0014	0.0014	0.0016	0.0020	0.0021	0.0023	0.0025	0.0027	0.0029	0.0031	0.0034	0.0038	0.0039	0.0042	0.0045
2.50	0.0033	0.0011	0.0013	0.0013	0.0015	0.0019	0.0020	0.0022	0.0024	0.0026	0.0028	0.0031	0.0033	0.0037	0.0038	0.0041	0.0044

Table 5. This table shows the levels in the atmosphere in which the data for each of the scans was taken.

Scans Taken in Each Atmospheric Layer

	April 8th	April 9th	April 12th	April 14th	April 19th A	April 19th B
Boundary Layer (< 300 m):	1…3	1…3	1, 2, 7, 13	1, 7	1, 4	1, 4
Mid-Troposphere (300 - 2000 m):		4, 7	5, 8…12, 14, 15	6, 10…14	3, 5, 6, 9	
Free Troposphere (> 2000 m):	7, 8	5, 6	3, 4	8, 9	7, 8	3

	April 23rd	April 25th A	April 25th B	April 28th	May 1st
Boundary Layer (< 300 m):	1, 10	1	1, 5, 11	1, 3	1
Mid-Troposphere (300 - 2000 m):	5…9	5…7	3, 6…9	5, 6	3…6
Free Troposphere (> 2000 m):	3	3, 4, 8, 9	4, 10	4, 7, 8	2, 7

Table 6. This table shows the number of scans for each group of cloud optical depths.

Number of Scans Per Optical Cloud Depth Category

Cloud Optical Depth:	1…19	20…49	50…100	100+
Cumulus:	34	31	7	15
Stratus:	82	5	0	0

Table 7. The following table shows the scan numbers, optical thicknesses, albedos, and mixing states for April 8th, 2001.

April 8th Scan Data

	Optical Depth:		**Albedo:**		**Mixing State:**
Scan #1:	Cumulus:	33	Cumulus:	0.81	Internal
	Stratus:	4	Stratus:	0.34	Internal
Scan #2:	Optical Depth:		Albedo:		
	Cumulus:	33	Cumulus:	0.81	Internal
	Stratus:	4	Stratus:	0.34	Internal
Scan #3:	Optical Depth:		Albedo:		
	Cumulus:	16	Cumulus:	0.68	External
	Stratus:	2	Stratus:	0.21	External
Scan #7:	Optical Depth:		Albedo:		
	Cumulus:	19	Cumulus:	0.71	Internal
	Stratus:	3	Stratus:	0.28	Internal
Scan #8:	Optical Depth:		Albedo:		
	Cumulus:	24	Cumulus:	0.76	Internal
	Stratus:	3	Stratus:	0.28	Internal

Table 8. The following table shows the scan numbers, optical thicknesses, albedos, and mixing states for April 9th, 2001.

April 9th Scan Data

	Optical Depth:		**Albedo:**		**Mixing State:**
Scan #1:	Cumulus:	43	Cumulus:	0.85	Internal
	Stratus:	6	Stratus:	0.44	Internal
Scan #2:	Optical Depth:		Albedo:		
	Cumulus:	45	Cumulus:	0.85	Internal
	Stratus:	6	Stratus:	0.44	Internal
Scan #3:	Optical Depth:		Albedo:		
	Cumulus:	232	Cumulus:	0.97	Internal
	Stratus:	31	Stratus:	0.80	Internal
Scan #4:	Optical Depth:		Albedo:		
	Cumulus:	16	Cumulus:	0.68	Internal
	Stratus:	2	Stratus:	0.21	Internal
Scan #5:	Optical Depth:		Albedo:		
	Cumulus:	21	Cumulus:	0.73	External
	Stratus:	3	Stratus:	0.28	External
Scan #6:	Optical Depth:		Albedo:		
	Cumulus:	19	Cumulus:	0.71	External
	Stratus:	3	Stratus:	0.28	External
Scan #7:	Optical Depth:		Albedo:		
	Cumulus:	25	Cumulus:	0.76	Internal
	Stratus:	3	Stratus:	0.28	Internal

Table 9. The following table shows the scan numbers, optical thicknesses, albedos, and mixing states for April 12th, 2001.

April 12th Scan Data

Scan #1:	**Optical Depth:**		**Albedo:**		**Mixing State:**
	Cumulus:	**87**	**Cumulus:**	0.92	External
	Stratus:	**12**	**Stratus:**	0.60	External
Scan #2:	**Optical Depth:**		**Albedo:**		
	Cumulus:	**328**	**Cumulus:**	0.98	External
	Stratus:	**44**	**Stratus:**	0.85	External
Scan #3:	**Optical Depth:**		**Albedo:**		
	Cumulus:	**18**	**Cumulus:**	0.70	Internal
	Stratus:	**2**	**Stratus:**	0.24	Internal
Scan #4:	**Optical Depth:**		**Albedo:**		
	Cumulus:	**21**	**Cumulus:**	0.73	Internal
	Stratus:	**3**	**Stratus:**	0.27	Internal
Scan #5:	**Optical Depth:**		**Albedo:**		
	Cumulus:	**42**	**Cumulus:**	0.85	Internal
	Stratus:	**6**	**Stratus:**	0.42	Internal
Scan #7:	**Optical Depth:**		**Albedo:**		
	Cumulus:	**41**	**Cumulus:**	0.84	Internal
	Stratus:	**5**	**Stratus:**	0.41	Internal
Scan #8:	**Optical Depth:**		**Albedo:**		
	Cumulus:	**58**	**Cumulus:**	0.88	Internal
	Stratus:	**8**	**Stratus:**	0.50	Internal
Scan #9:	**Optical Depth:**		**Albedo:**		
	Cumulus:	**41**	**Cumulus:**	0.84	Internal
	Stratus:	**5**	**Stratus:**	0.41	Internal
Scan #10:	**Optical Depth:**		**Albedo:**		
	Cumulus:	**90**	**Cumulus:**	0.92	External
	Stratus:	**12**	**Stratus:**	0.61	External
Scan #11:	**Optical Depth:**		**Albedo:**		
	Cumulus:	**118**	**Cumulus:**	0.94	External
	Stratus:	**16**	**Stratus:**	0.67	External
Scan #12:	**Optical Depth:**		**Albedo:**		
	Cumulus:	**151**	**Cumulus:**	0.95	External
	Stratus:	**20**	**Stratus:**	0.73	External
Scan #13:	**Optical Depth:**		**Albedo:**		
	Cumulus:	**87**	**Cumulus:**	0.92	External
	Stratus:	**12**	**Stratus:**	0.60	External
Scan #14:	**Optical Depth:**		**Albedo:**		
	Cumulus:	**104**	**Cumulus:**	0.93	External
	Stratus:	**14**	**Stratus:**	0.64	External
Scan #15:	**Optical Depth:**		**Albedo:**		
	Cumulus:	**118**	**Cumulus:**	0.94	Internal
	Stratus:	**16**	**Stratus:**	0.67	Internal

Table 10. The following table shows the scan numbers, optical thicknesses, albedos, and mixing states for April 14th, 2001.

April 14th Scan Data

	Optical Depth:		**Albedo:**		**Mixing State:**
Scan #1:	Cumulus:	107	Cumulus:	0.93	External
	Stratus:	14	Stratus:	0.65	External
Scan #7:	Optical Depth:		Albedo:		
	Cumulus:	62	Cumulus:	0.89	External
	Stratus:	8	Stratus:	0.52	External
Scan #8:	Optical Depth:		Albedo:		
	Cumulus:	130	Cumulus:	0.94	External
	Stratus:	17	Stratus:	0.69	External
Scan #9:	Optical Depth:		Albedo:		
	Cumulus:	131	Cumulus:	0.94	External
	Stratus:	18	Stratus:	0.70	External
Scan #10:	Optical Depth:		Albedo:		
	Cumulus:	142	Cumulus:	0.95	External
	Stratus:	19	Stratus:	0.71	External
Scan #11:	Optical Depth:		Albedo:		
	Cumulus:	120	Cumulus:	0.94	Internal
	Stratus:	16	Stratus:	0.68	Internal
Scan #12:	Optical Depth:		Albedo:		
	Cumulus:	72	Cumulus:	0.90	External
	Stratus:	10	Stratus:	0.56	External
Scan #13:	Optical Depth:		Albedo:		
	Cumulus:	137	Cumulus:	0.95	External
	Stratus:	18	Stratus:	0.71	External
Scan #14:	Optical Depth:		Albedo:		
	Cumulus:	154	Cumulus:	0.95	External
	Stratus:	21	Stratus:	0.73	External

Table 11. The following table shows the scan numbers, optical thicknesses, albedos, and mixing states for April 19th, 2001 A.

April 19th A Albedos

	Optical Depth:		**Albedo:**		**Mixing State:**
Scan #1:	Cumulus:	12	Cumulus:	0.61	Internal
	Stratus:	2	Stratus:	0.21	Internal
Scan #3:	Optical Depth:		Albedo:		
	Cumulus:	21	Cumulus:	0.73	Internal
	Stratus:	3	Stratus:	0.28	Internal
Scan #4:	Optical Depth:		Albedo:		
	Cumulus:	21	Cumulus:	0.73	Internal
	Stratus:	3	Stratus:	0.28	Internal
Scan #5:	Optical Depth:		Albedo:		
	Cumulus:	13	Cumulus:	0.63	Internal
	Stratus:	2	Stratus:	0.21	Internal
Scan #6:	Optical Depth:		Albedo:		
	Cumulus:	17	Cumulus:	0.69	Internal
	Stratus:	2	Stratus:	0.21	Internal
Scan #7:	Optical Depth:		Albedo:		
	Cumulus:	19	Cumulus:	0.71	Internal
	Stratus:	3	Stratus:	0.28	Internal
Scan #8:	Optical Depth:		Albedo:		
	Cumulus:	13	Cumulus:	0.63	Internal
	Stratus:	2	Stratus:	0.21	Internal
Scan #9:	Optical Depth:		Albedo:		
	Cumulus:	13	Cumulus:	0.63	Internal
	Stratus:	2	Stratus:	0.21	Internal

Table 12. The following table shows the scan numbers, optical thicknesses, albedos, and mixing states for April 19th, 2001 B.

April 19th B Scan Data

Scan #1:	**Optical Depth:**		**Albedo:**		**Mixing State:**
	Cumulus:	72	Cumulus:	0.90	External
	Stratus:	10	Stratus:	0.56	External
Scan #3:	Optical Depth:		Albedo:		
	Cumulus:	11	Cumulus:	0.59	Internal
	Stratus:	1	Stratus:	0.11	Internal
Scan #4:	Optical Depth:		Albedo:		
	Cumulus:	14	Cumulus:	0.65	Internal
	Stratus:	2	Stratus:	0.21	Internal

Table 13. The following table shows the scan numbers, optical thicknesses, albedos, and mixing states for April 23rd, 2001.

April 23rd Scan Data

	Optical Depth:		**Albedo:**		**Mixing State:**
Scan #1:	Cumulus:	13	Cumulus:	0.63	Internal
	Stratus:	2	Stratus:	0.21	Internal
Scan #3:	Optical Depth:		Albedo:		
	Cumulus:	15	Cumulus:	0.66	Internal
	Stratus:	2	Stratus:	0.21	Internal
Scan #5:	Optical Depth:		Albedo:		
	Cumulus:	19	Cumulus:	0.71	Internal
	Stratus:	3	Stratus:	0.28	Internal
Scan #6:	Optical Depth:		Albedo:		
	Cumulus:	19	Cumulus:	0.71	Internal
	Stratus:	3	Stratus:	0.28	Internal
Scan #7:	Optical Depth:		Albedo:		
	Cumulus:	22	Cumulus:	0.74	Internal
	Stratus:	3	Stratus:	0.28	Internal
Scan #8:	Optical Depth:		Albedo:		
	Cumulus:	17	Cumulus:	0.69	Internal
	Stratus:	2	Stratus:	0.21	Internal
Scan #9:	Optical Depth:		Albedo:		
	Cumulus:	19	Cumulus:	0.71	Internal
	Stratus:	2	Stratus:	0.21	Internal
Scan #10:	Optical Depth:		Albedo:		
	Cumulus:	20	Cumulus:	0.72	Internal
	Stratus:	3	Stratus:	0.28	Internal

Table 14. The following table shows the scan numbers, optical thicknesses, albedos, and mixing states for April 25th, 2001 A.

April 25th A Scan Data

	Optical Depth:		**Albedo:**		**Mixing State:**
Scan #1:	Cumulus:	37	Cumulus:	0.83	Internal
	Stratus:	5	Stratus:	0.39	Internal
Scan #3:	Optical Depth:		Albedo:		
	Cumulus:	7	Cumulus:	0.48	Internal
	Stratus:	1	Stratus:	0.11	Internal
Scan #4:	Optical Depth:		Albedo:		
	Cumulus:	17	Cumulus:	0.69	Internal
	Stratus:	2	Stratus:	0.21	Internal
Scan #5:	Optical Depth:		Albedo:		
	Cumulus:	17	Cumulus:	0.69	Internal
	Stratus:	2	Stratus:	0.21	Internal
Scan #6:	Optical Depth:		Albedo:		
	Cumulus:	19	Cumulus:	0.71	Internal
	Stratus:	3	Stratus:	0.28	Internal
Scan #7:	Optical Depth:		Albedo:		
	Cumulus:	17	Cumulus:	0.69	Internal
	Stratus:	2	Stratus:	0.21	Internal
Scan #8:	Optical Depth:		Albedo:		
	Cumulus:	15	Cumulus:	0.66	Internal
	Stratus:	2	Stratus:	0.21	Internal
Scan #9:	Optical Depth:		Albedo:		
	Cumulus:	13	Cumulus:	0.63	Internal
	Stratus:	2	Stratus:	0.21	Internal

Table 15. The following table shows the scan numbers, optical thicknesses, albedos, and mixing states for April 25th, 2001 B.

April 25th B Scan Data

	Optical Depth:		**Albedo:**		**Mixing State:**
Scan #1:	Cumulus:	34	Cumulus:	0.82	Internal
	Stratus:	5	Stratus:	0.39	Internal
Scan #3:	Optical Depth:		Albedo:		
	Cumulus:	27	Cumulus:	0.78	Internal
	Stratus:	4	Stratus:	0.34	Internal
Scan #4:	Optical Depth:		Albedo:		
	Cumulus:	15	Cumulus:	0.66	Internal
	Stratus:	2	Stratus:	0.21	Internal
Scan #5:	Optical Depth:		Albedo:		
	Cumulus:	20	Cumulus:	0.72	Internal
	Stratus:	3	Stratus:	0.28	Internal
Scan #6:	Optical Depth:		Albedo:		
	Cumulus:	23	Cumulus:	0.75	Internal
	Stratus:	3	Stratus:	0.28	Internal
Scan #7:	Optical Depth:		Albedo:		
	Cumulus:	21	Cumulus:	0.73	Internal
	Stratus:	3	Stratus:	0.28	Internal
Scan #8:	Optical Depth:		Albedo:		
	Cumulus:	22	Cumulus:	0.74	Internal
	Stratus:	3	Stratus:	0.28	Internal
Scan #9:	Optical Depth:		Albedo:		
	Cumulus:	22	Cumulus:	0.74	Internal
	Stratus:	3	Stratus:	0.28	Internal
Scan #10:	Optical Depth:		Albedo:		
	Cumulus:	13	Cumulus:	0.63	Internal
	Stratus:	2	Stratus:	0.21	Internal
Scan #11:	Optical Depth:		Albedo:		
	Cumulus:	20	Cumulus:	0.72	Internal
	Stratus:	3	Stratus:	0.28	Internal

Table 16. The following table shows the scan numbers, optical thicknesses, albedos, and mixing states for April 28th, 2001.

April 28th Scan Data

	Optical Depth:		**Albedo:**		**Mixing State:**
Scan #1:	Cumulus:	34	Cumulus:	0.82	Internal
	Stratus:	5	Stratus:	0.39	Internal
Scan #3:	Optical Depth:		Albedo:		
	Cumulus:	13	Cumulus:	0.63	Internal
	Stratus:	2	Stratus:	0.21	Internal
Scan #4:	Optical Depth:		Albedo:		
	Cumulus:	14	Cumulus:	0.65	Internal
	Stratus:	2	Stratus:	0.21	Internal
Scan #5:	Optical Depth:		Albedo:		
	Cumulus:	21	Cumulus:	0.73	Internal
	Stratus:	3	Stratus:	0.28	Internal
Scan #6:	Optical Depth:		Albedo:		
	Cumulus:	24	Cumulus:	0.76	Internal
	Stratus:	3	Stratus:	0.28	Internal
Scan #7:	Optical Depth:		Albedo:		
	Cumulus:	20	Cumulus:	0.72	External
	Stratus:	3	Stratus:	0.28	External
Scan #8:	Optical Depth:		Albedo:		
	Cumulus:	16	Cumulus:	0.68	Internal
	Stratus:	2	Stratus:	0.21	Internal

Table 17. The following table shows the scan numbers, optical thicknesses, albedos, and mixing states for May 1st, 2001.

May 1st Scan Data

	Optical Depth:		**Albedo:**		**Mixing State:**
Scan #1:	Cumulus:	25	Cumulus:	0.76	External
	Stratus:	3	Stratus:	0.28	External
Scan #2:	Optical Depth:		Albedo:		
	Cumulus:	157	Cumulus:	0.95	External
	Stratus:	21	Stratus:	0.73	External
Scan #3:	Optical Depth:		Albedo:		
	Cumulus:	17	Cumulus:	0.69	Internal
	Stratus:	2	Stratus:	0.21	Internal
Scan #4:	Optical Depth:		Albedo:		
	Cumulus:	21	Cumulus:	0.73	Internal
	Stratus:	3	Stratus:	0.28	Internal
Scan #5:	Optical Depth:		Albedo:		
	Cumulus:	20	Cumulus:	0.72	Internal
	Stratus:	3	Stratus:	0.28	Internal
Scan #6:	Optical Depth:		Albedo:		
	Cumulus:	19	Cumulus:	0.71	Internal
	Stratus:	3	Stratus:	0.28	Internal
Scan #7:	Optical Depth:		Albedo:		
	Cumulus:	16	Cumulus:	0.68	Internal
	Stratus:	2	Stratus:	0.21	Internal

Table 18. This is an albedo frequency chart for all the scans combined, indicating the number of scans that correlate to each range of albedo values. See Figure 11 for a graph of this chart.

Albedo Frequency Chart

	10...19	20...29	30...39	40...49	50...59	60...69	70...79	80...89	90...100
Cumulus:	0	0	0	1	1	23	31	12	19
Stratus:	2	53	6	5	4	9	6	2	0

Table 19. The chart shows the frequency of scan albedos for cumulus and stratus clouds, for both internally and externally mixed aerosols. For a graphical representation see Figure 12.

Albedo Frequency Chart - Externally Mixed

	10…19	20…29	30…39	40…49	50…59	60…69	70…79	80…89	90…100
Cumulus:	0	0	0	0	0	1	4	1	17
Stratus:	0	5	0	0	3	7	6	1	0

Albedo Frequency Chart - Internally Mixed

	10…19	20…29	30…39	40…49	50…59	60…69	70…79	80…89	90…100
Cumulus:	0	0	0	1	1	21	27	11	3
Stratus:	2	48	6	5	1	2	0	1	0

Table 20. This table shows the range in Sc values for each of the dry aerosol particle sizes for the scans taken in the boundary layer (<300 m).

Sc Ranges for Each Dry Particle Size for the Boundary Layer

Particle Size (Dp):	Sc (%):
0.040	0.5 - 2.5
0.059	0.28 - 2.0
0.086	0.14 - 0.9
0.126	0.006 - 0.2
0.186	0.0009 - 0.1
0.273	0.0005 - 0.05
0.400	0.00006 - 0.01

Table 21. This table shows the range in Sc values for each of the dry aerosol particle sizes for the scans taken in the pollution layer (300 m to 2,000 m).

Sc Ranges for Each Dry Particle Size for the Pollution Layer

Particle Size (Dp):	Sc (%):
0.040	0.45 - 1.2
0.059	0.2 - 1.5
0.086	0.08 - 0.4
0.126	0.003 - 0.22
0.186	0.0005 - 0.2
0.273	0.0001 - 0.19
0.400	0.00005 - 0.18

Table 22. This table shows the range in Sc values for each of the dry aerosol particle sizes for the scans taken in the free troposphere layer (>2,000 m).

Sc Ranges for Each Dry Particle Size for the Free Troposphere Layer

Particle Size (Dp):	Sc (%):
0.040	0.45 - 2.5
0.059	0.25 - 1
0.086	0.15 - 0.5
0.126	0.08 - 0.4
0.186	0.02 - 0.2
0.273	0.002 - 0.008
0.400	0.0005 - 0.001

APPENDIX B

FIGURES

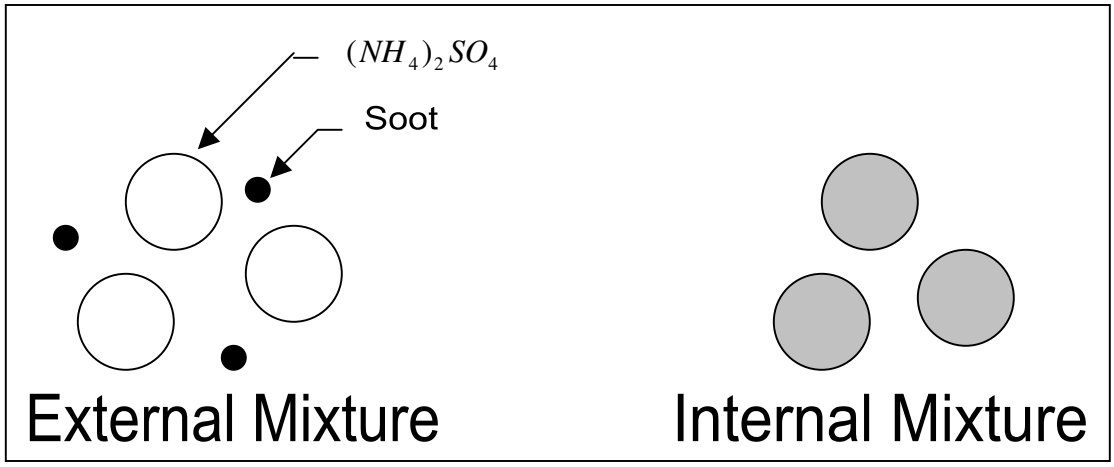

Figure 1. Mixing states of an aerosol-internal and external mixtures of $(NH_4)_2$ SO_4 and soot. (Seinfeld and Pandis, 1998)

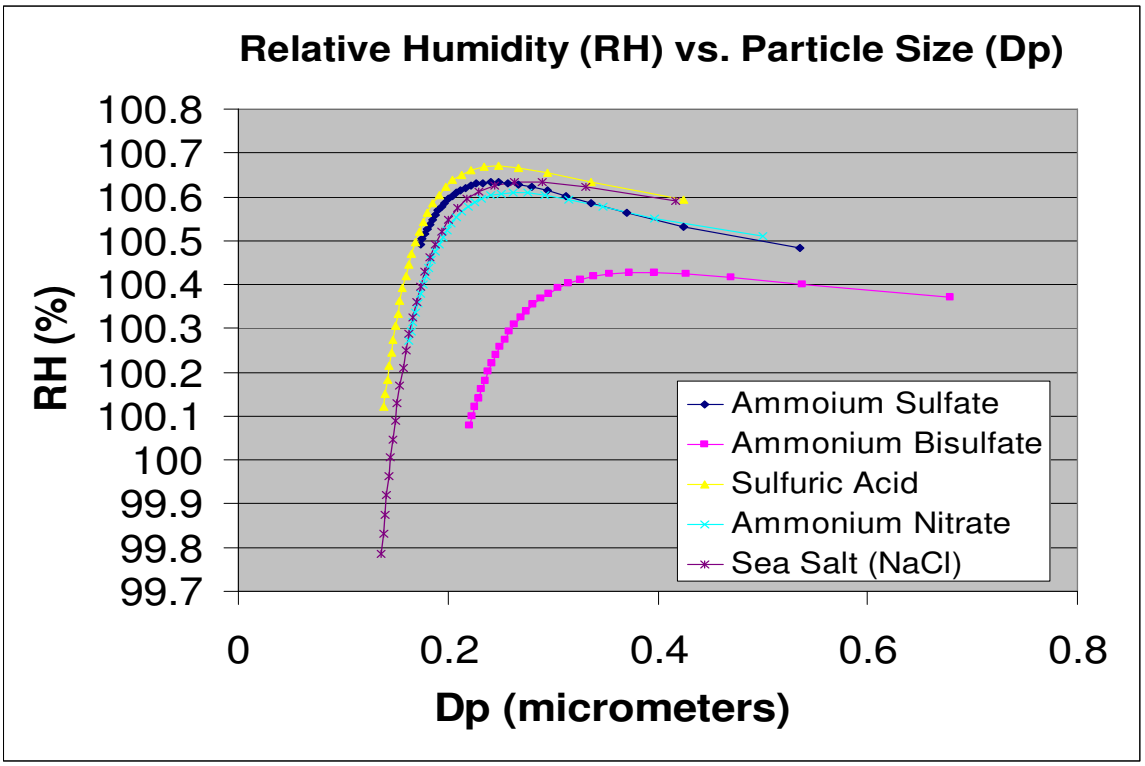

Figure 2. These are the Köhler curves for each of the substances considered in this study.

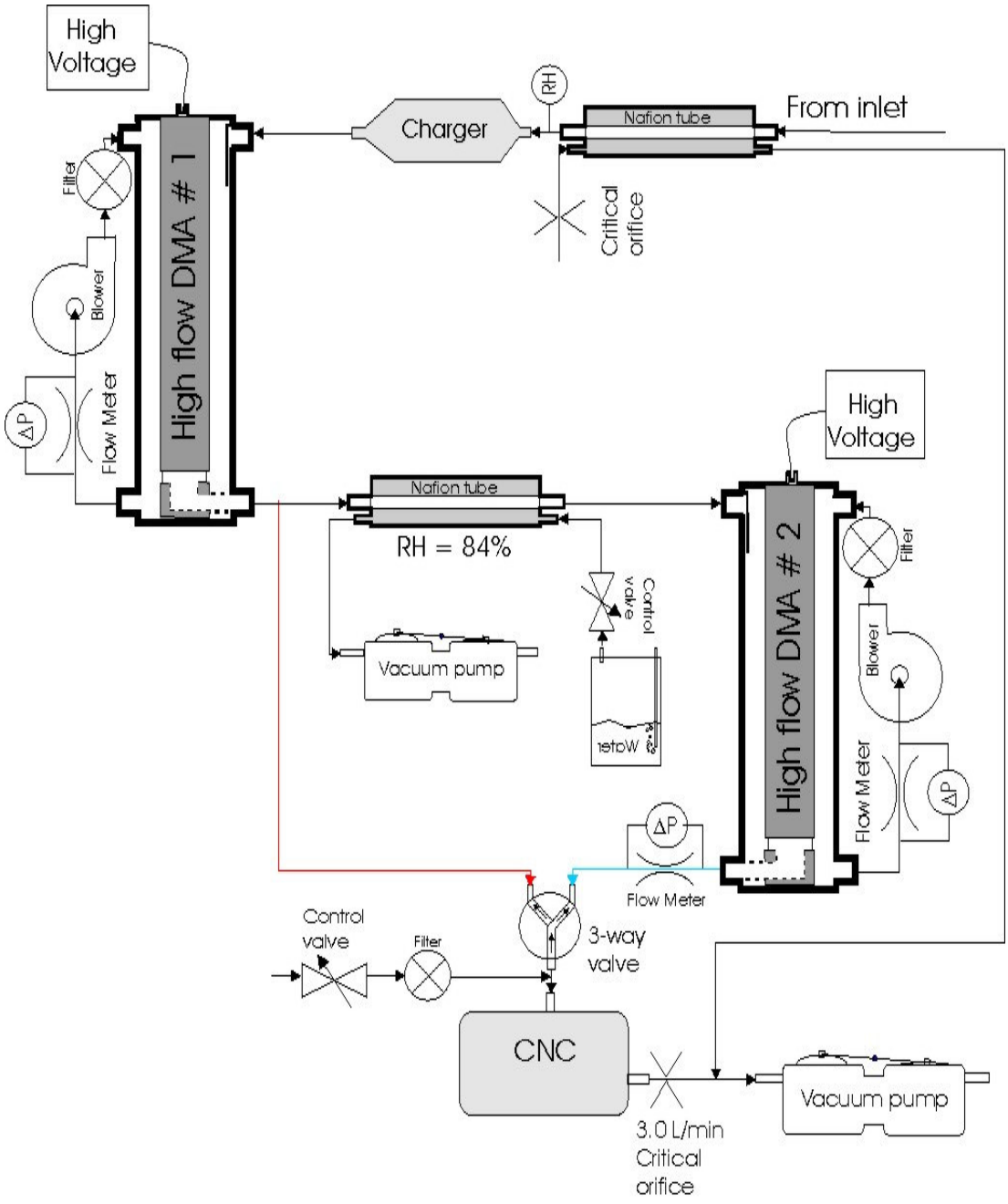

Figure 3. Schematic of the system mounted on the aircraft used during ACE-Asia. (From Collins, 2002)

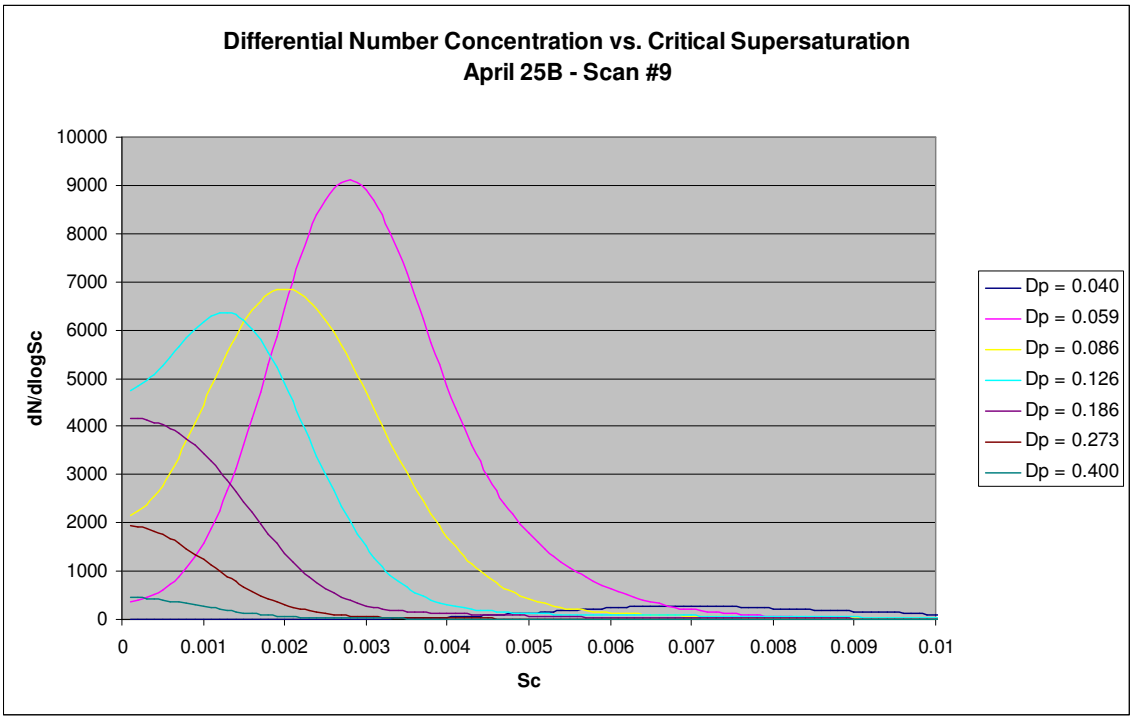

Figure 4. This graph of differential number concentration versus critical supersaturation is indicative of an internally mixed aerosol with single-peak distributions.

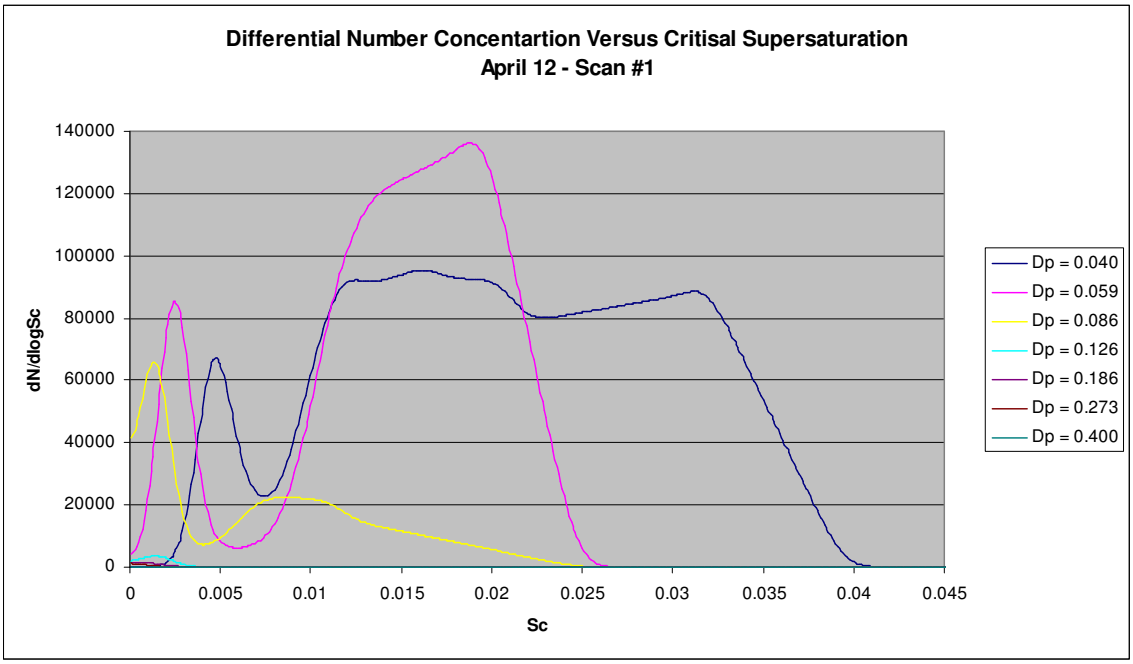

Figure 5. This graph of differential number concentration versus critical supersaturation is indicative of an externally mixed aerosol with multiple peaks in the distributions for particles with diameters equal to 0.040µm, 0.059µm, and 0.086µm.

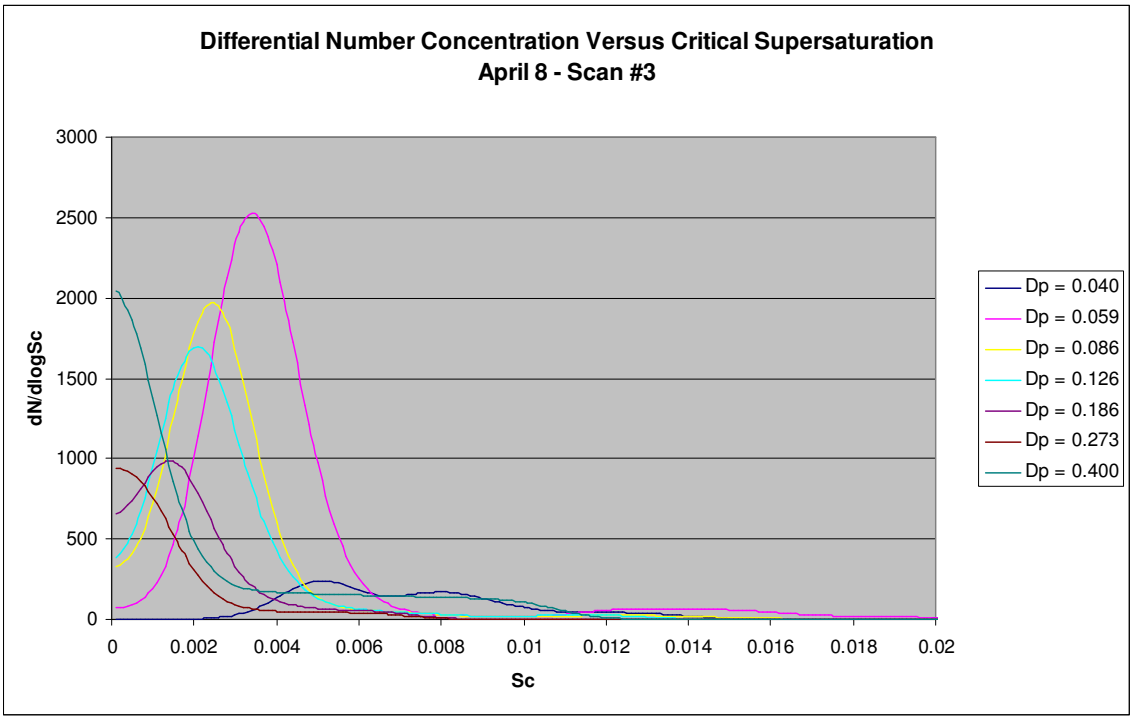

Figure 6. This graph of differential number concentration versus critical supersaturation is an example of an aerosol sample containing external mixtures for particles equal to 0.126 μm and smaller. The distribution for 0.059 μm particles has the most prevalent bi-modal distribution.

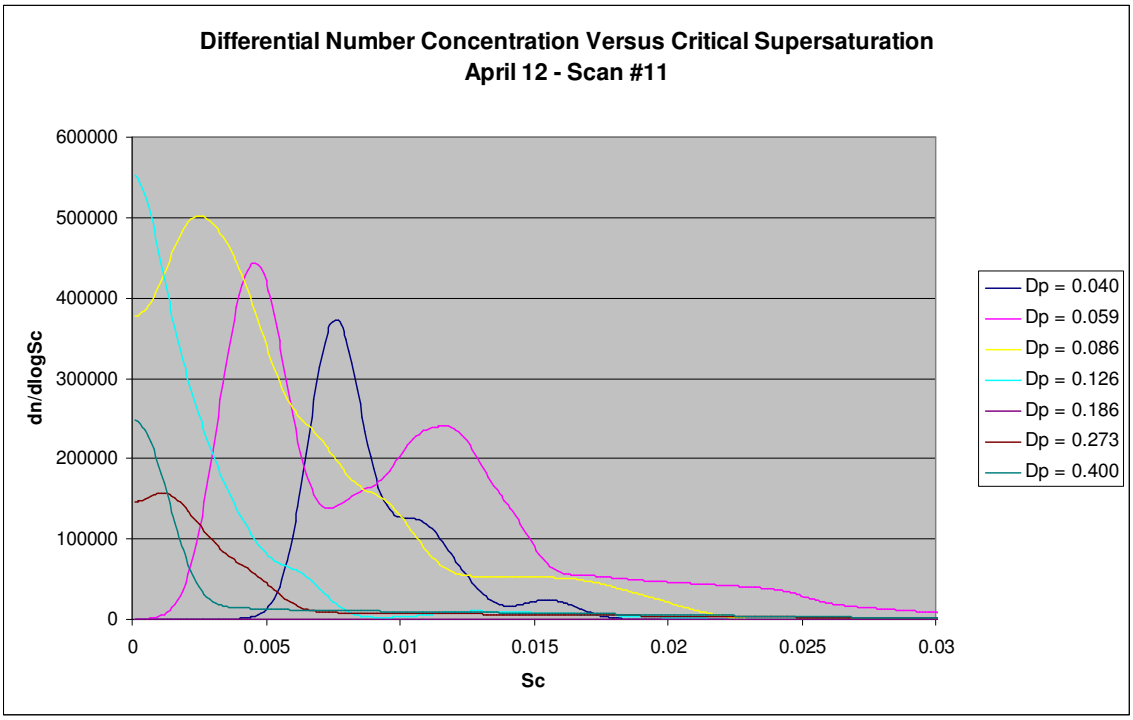

Figure 7. Same as Figure 6, with the 0.059 µm particle distribution remaining the most prevalent.

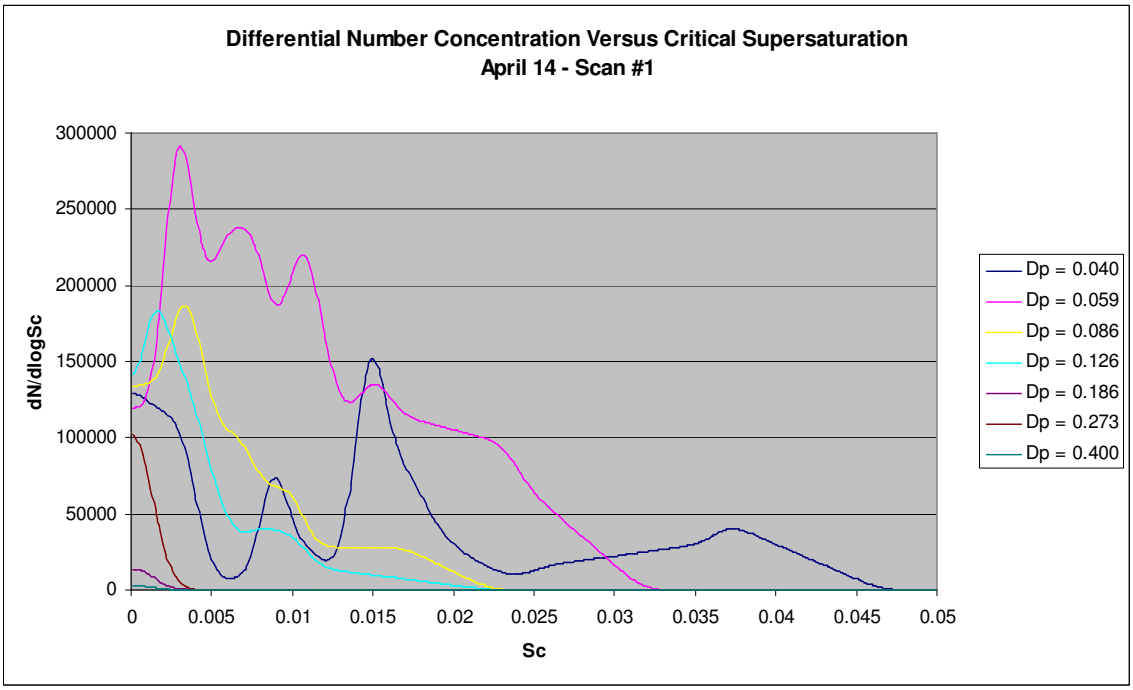

Figure 8. Same as Figure 6 with 0.040 µm particle distribution becoming the most prevalent.

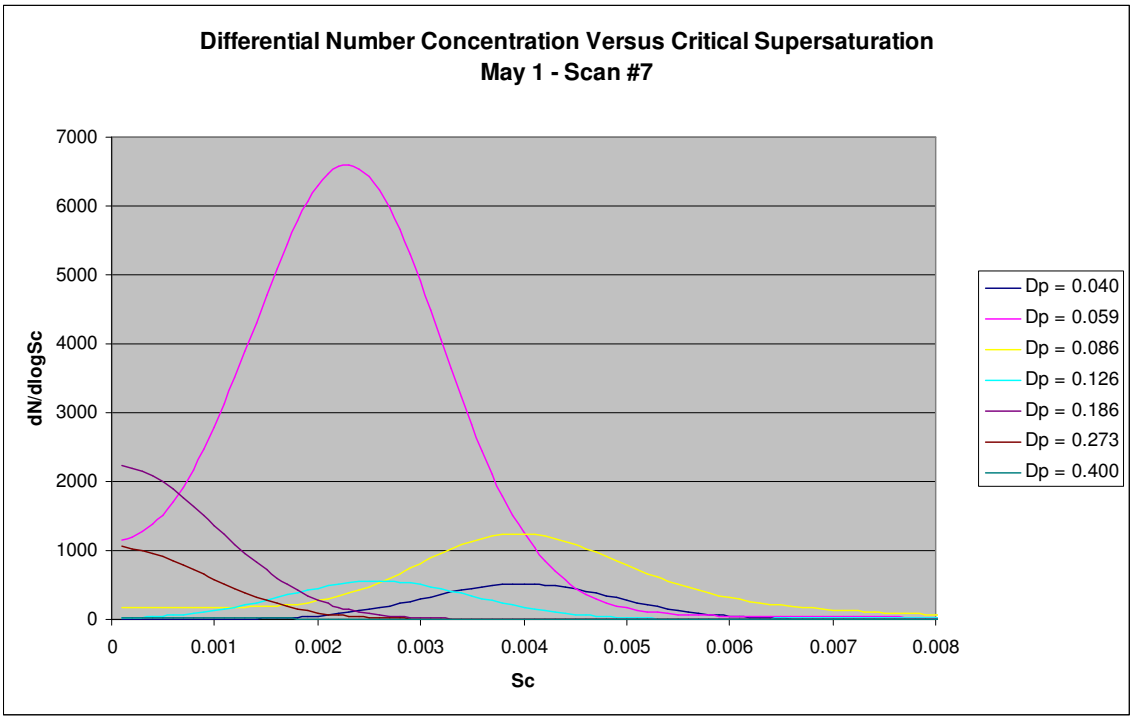

Figure 9. This graph shows the exception to most analyzed in this study, where the peak in a larger particle distribution correlates to a higher Sc than some smaller particles. In this example, the 0.059µm distribution peaks at 0.0023 while the 0.086µm distribution peaks at 0.004 and the 0.126µm distribution peaks at 0.0025.

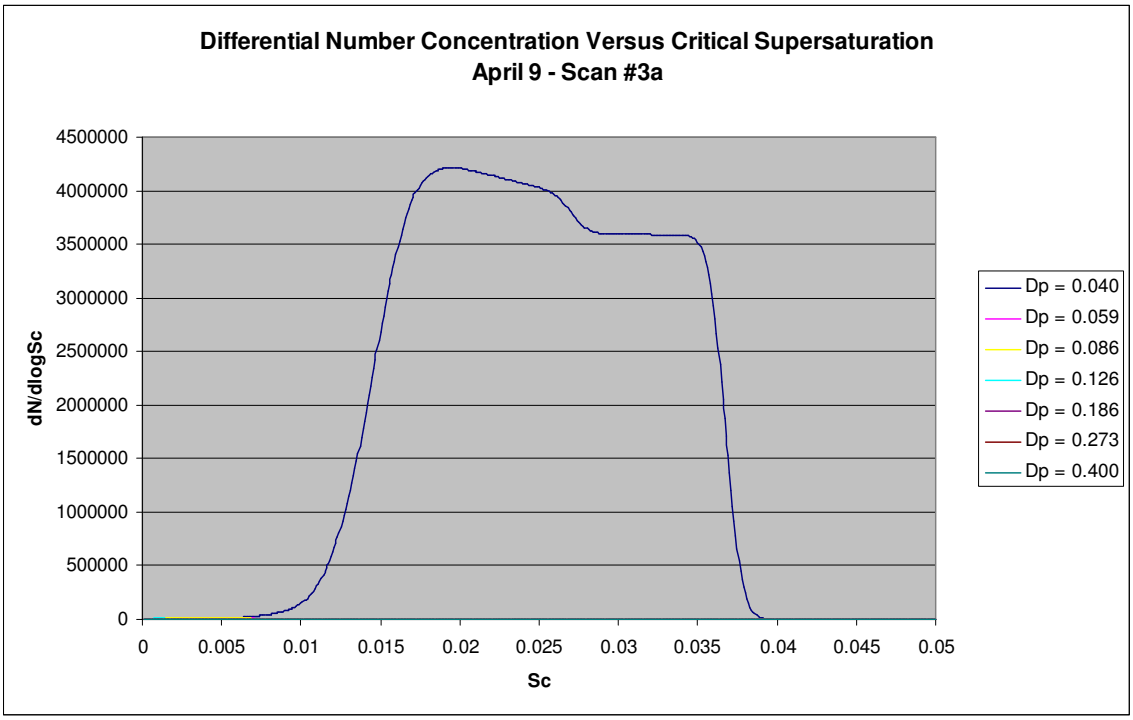

Figure 10. This graph of differential number concentration versus critical supersaturation demonstrates a dominant distribution. In this case, the distribution for 0.040 µm particles far exceeds the others peaking with counts near 4,200,000, while the other distributions peak below 12,000 counts (see Figure 11).

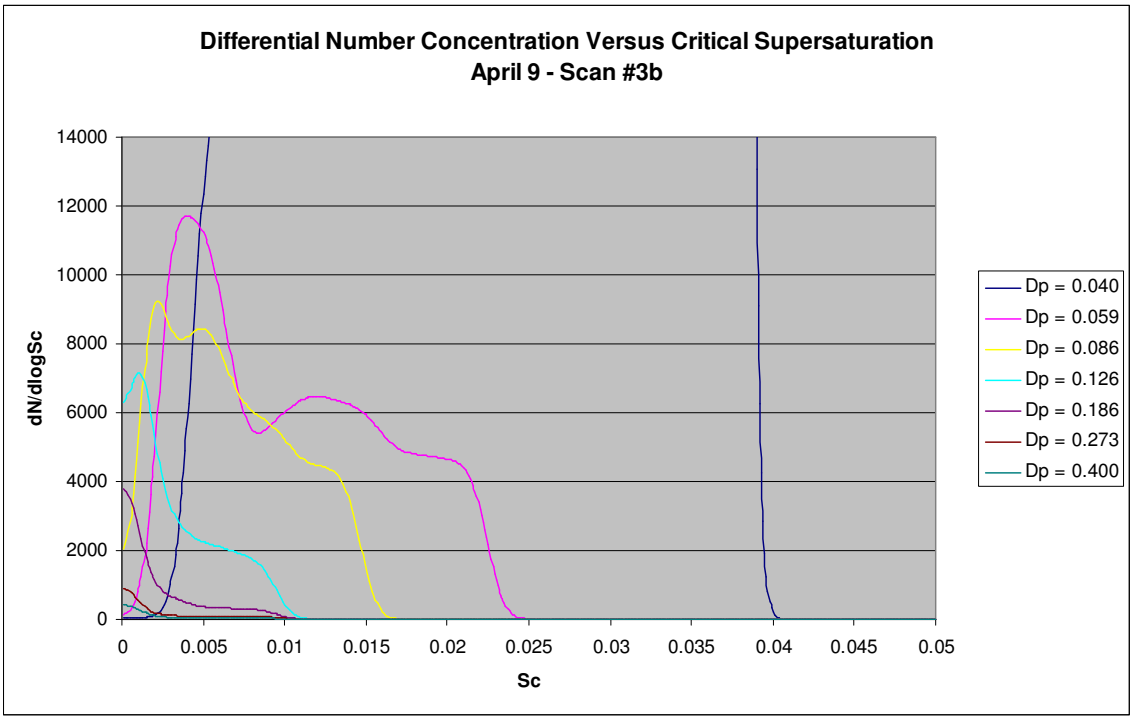

Figure 11. This graph of differential number concentration versus critical supersaturation shows the less dominant distributions for Figure 10. The 0.059 and 0.086 µm distributions show slightly bi-modal distributions, while the others appear more uni-modal.

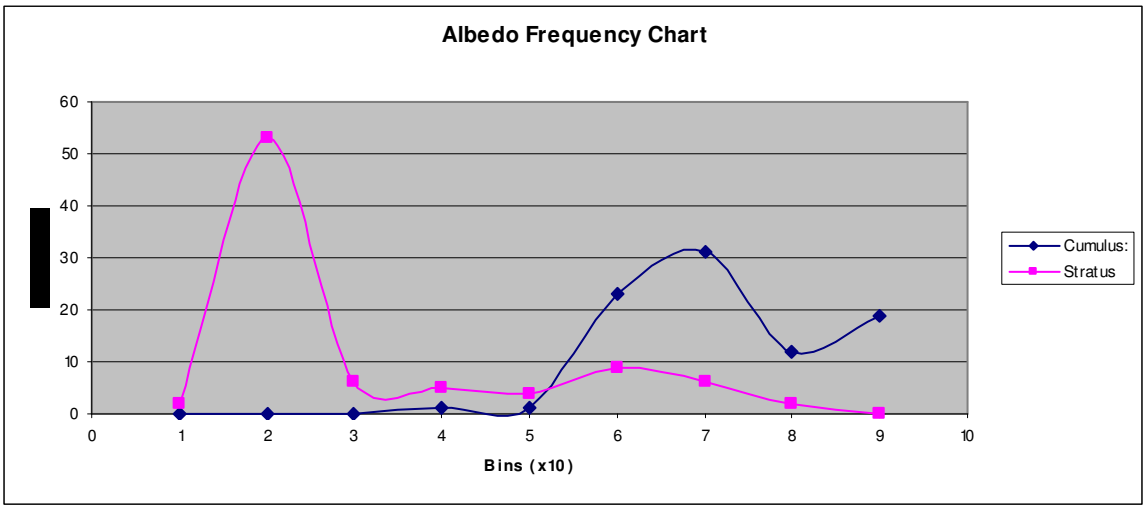

Figure 12. This graph displays the frequency of scans for each grouping of albedo values for both cumulus and stratus clouds. See Table 18 for the associated data chart. Clearly shown is a tendency for cumulus albedos to be high and stratus albedos to be low. (Note: 1 represents values 10-19, 2 represents 20-29, etc.)

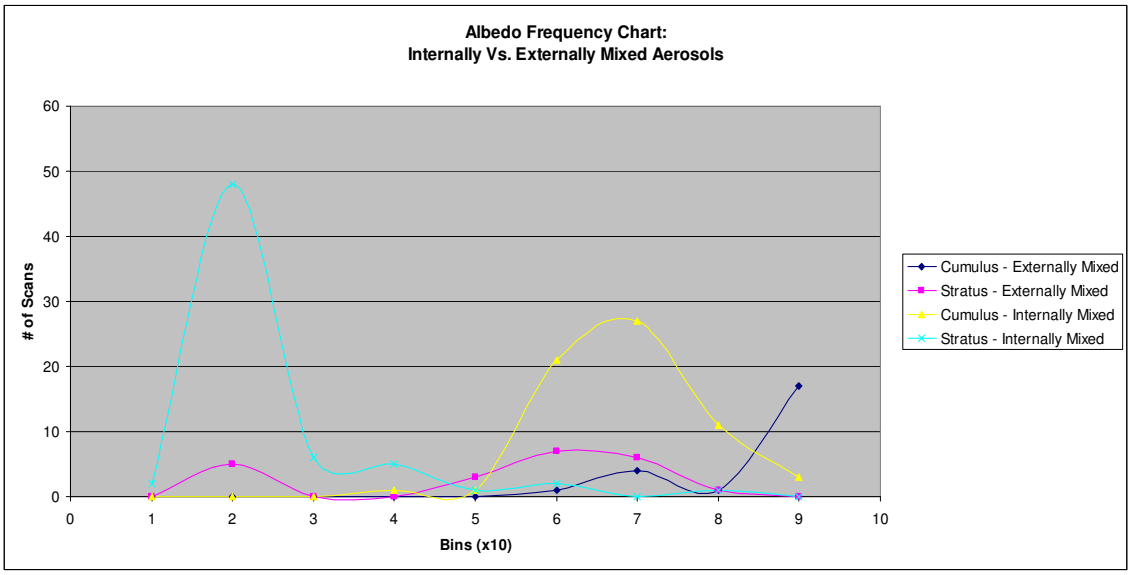

Figure 13. This graph displays the frequency of scans for each grouping of albedo values for cumulus and stratus clouds, both internally mixed and externally mixed scenerios. See Table 19 for the associated data chart. Both internally and externally mixed cumulus cloud albedos tend to be > 50, while there is a shift in the stratus cloud albedos from low values associated with internal mixtures to greater frequency of high values associated with external mixtures. (Note: 1 represents values 10-19, 2 represents 20-29, etc.)

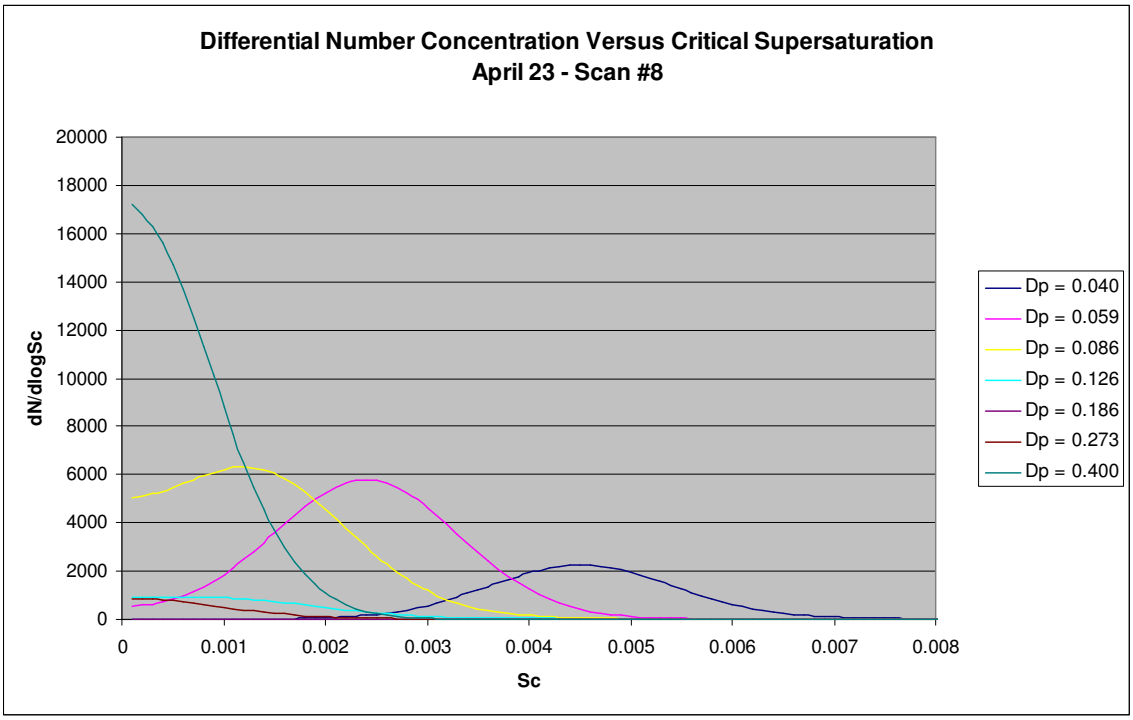

Figure 14. This graph of differential number concentration versus critical supersaturation shows a significant distribution of large (Dp = 0.400 μm) particles that resulted in a reduced cloud albedo values.

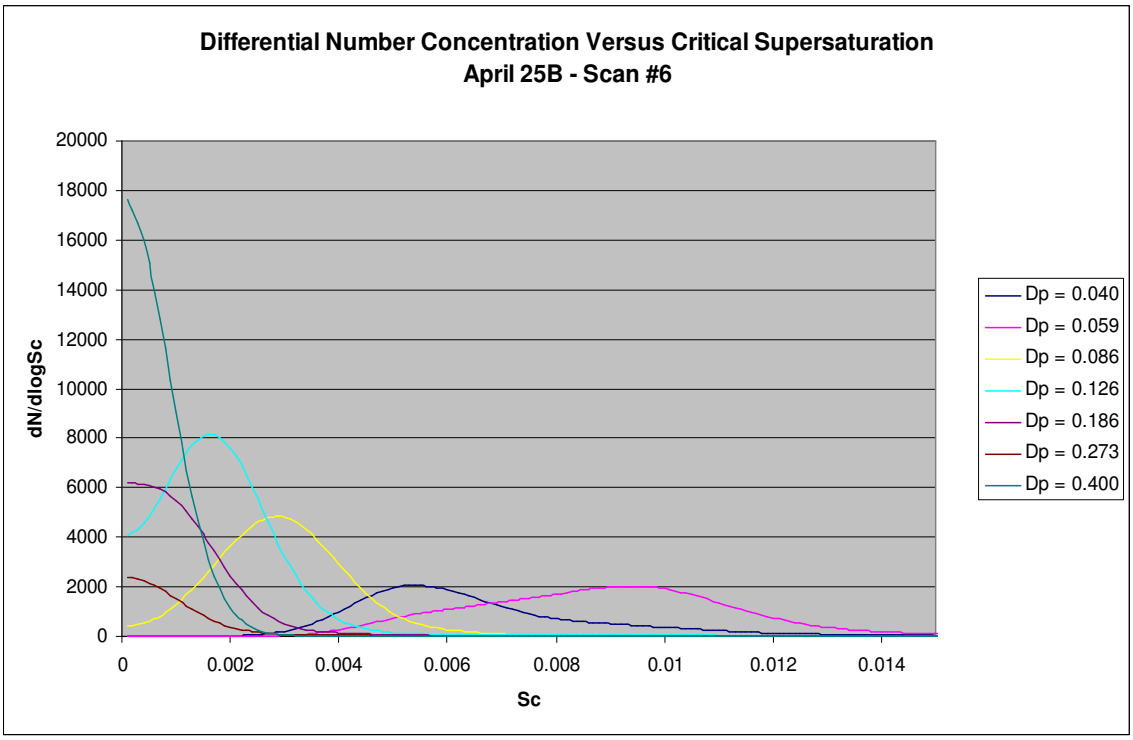

Figure 15. This graph of differential number concentration versus critical supersaturation shows a significant distribution of large (Dp = 0.400 µm) particles that did not result in reduced cloud albedo values, as in Figure 14. This particular scan also has 0.059 µm particles with higher Sc values than 0.040 µm particles.

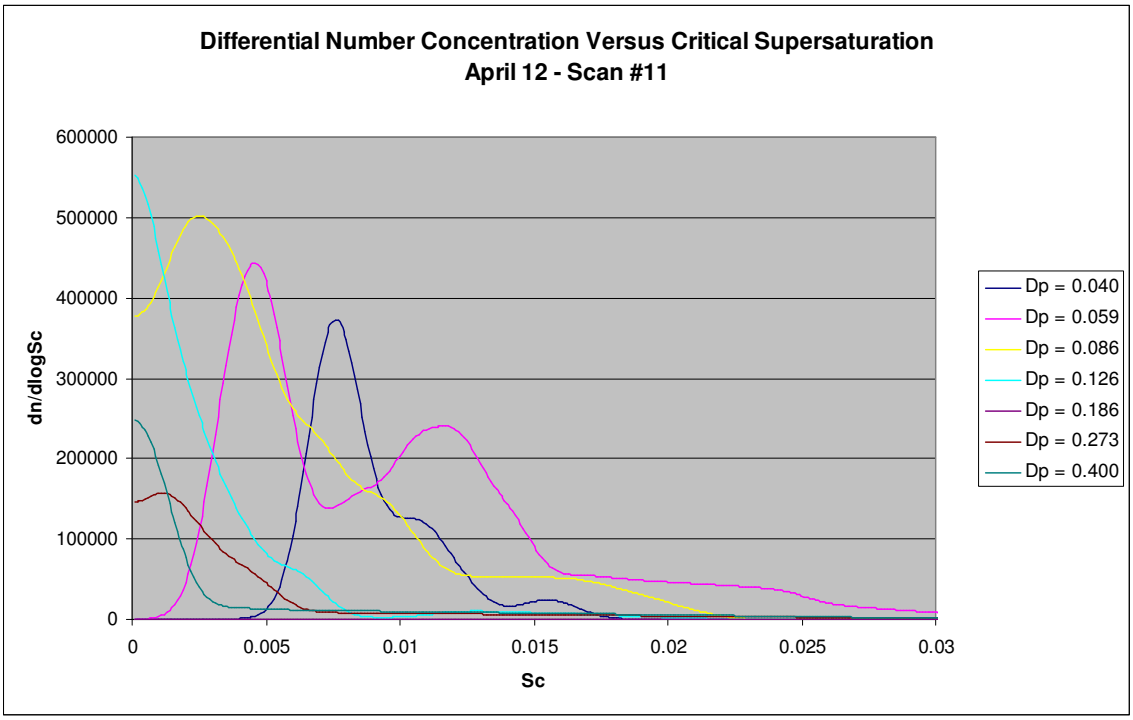

Figure 16. This graph of differential number concentration versus critical supersaturation shows an external mixture for the 0.059 μm particles with very high count values across all the particles sizes. This resulted in high cloud albedo values.

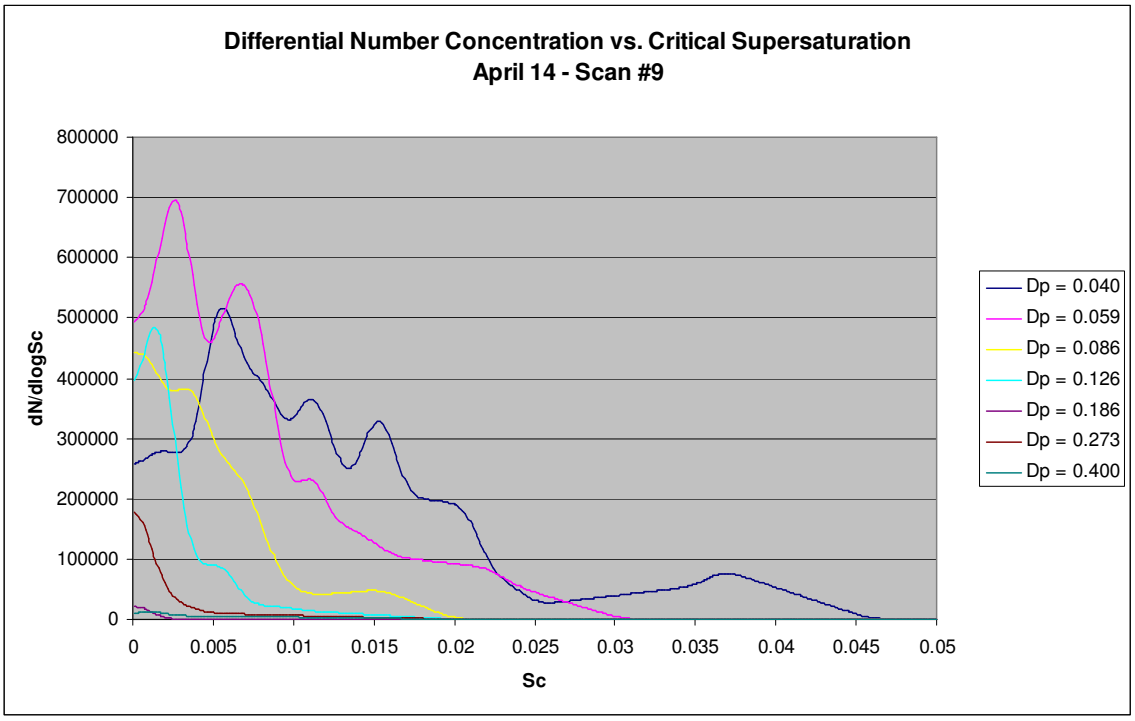

Figure 17. Same as Figure 16, except on a different date. The noise in the data for this plot is also observed to be much higher indicated by the multitude of peaks in the distributions.

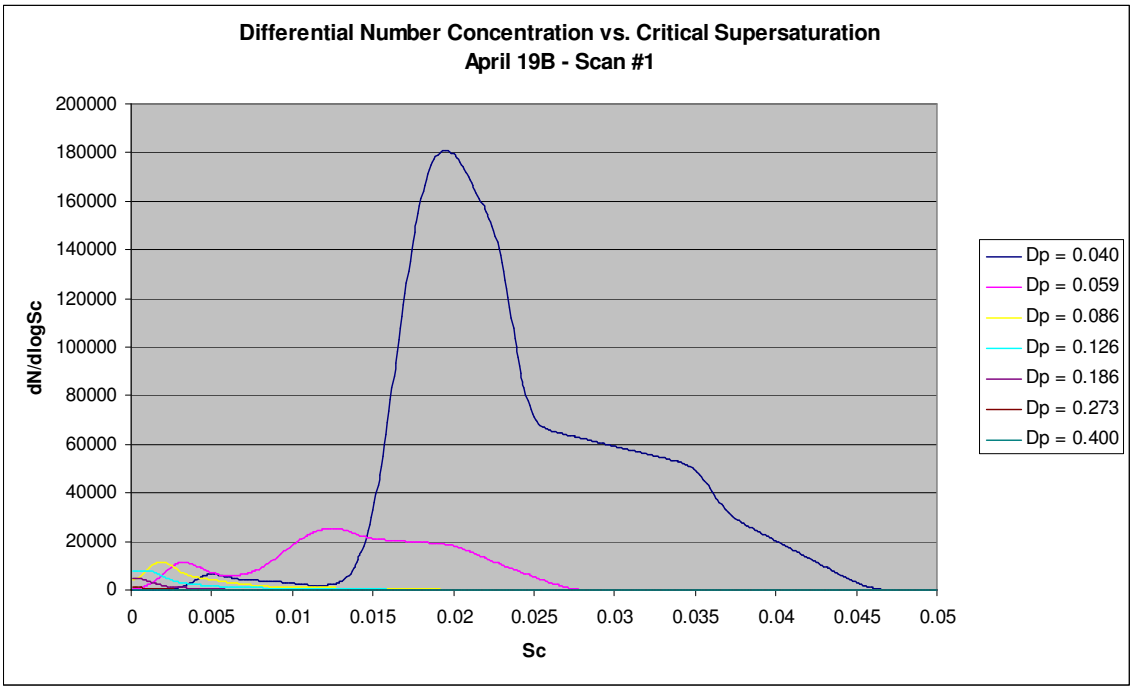

Figure 18. This is the distribution graph for April 19th B, taken 9:45 am at 162 meters above sea level. When compared to Figure 19, an elevated pollution layer can be observed as 0.040 µm particle concentration decreases along with associated Sc values.

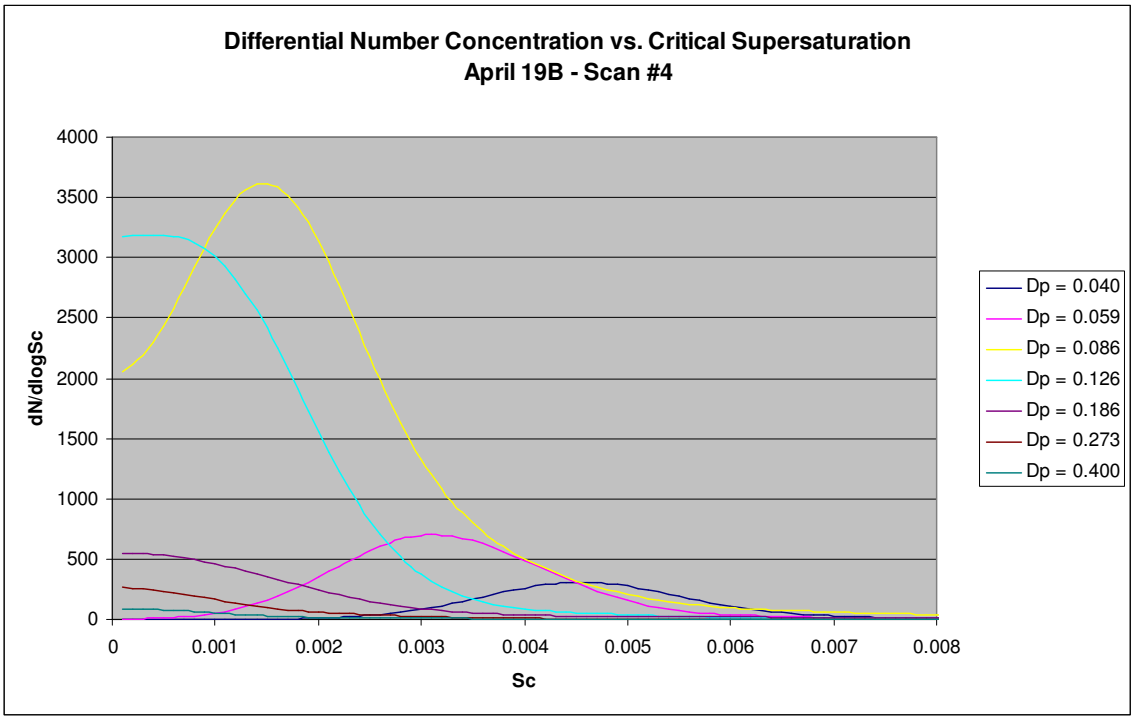

Figure 19. This is the distribution graph for April 19th B, taken 11:35 am at 120 meters above sea level. When compared to Figure 18, an elevated pollution layer can be observed as particle concentration increases along with associated Sc value

VITA

Timothy William Thomas was born in Rochester, New York. In 1995 he graduated from North Rose-Wolcott High School (Wolcott, NY) and acquired his Bachelor of Science Degree in Meteorology from the State University of New York (SUNY) at Oswego in 1999, when he also lead the North Rose-Wolcott Girls Varsity Volleyball team to the league championship victory as well as the SUNY Oswego Men's Volleyball team to a 2nd place Bronze Division finish at the USA National Tournament.

He continued his education at Texas A&M University working towards a Master's Degree in Atmospheric Sciences, where he became an active member and team leader of the TAMMSSDA storm chasing group. During his third year of studies he was offered teaching and coaching positions back in New York. He accepted the positions as a High School Earth Science Teacher and Boys Varsity Volleyball Coach at North Rose-Wolcott High School, his alma mater. He is currently still teaching earth science, along with coaching the Boys Varsity Volleyball Team and Boys JV Tennis Team at North Rose Wolcott HS. He also owns one of the largest disc jockey services in Rochester, NY: The Excellerator DJ Service. When not in the classroom, Mr. Thomas enjoys salmon fishing on Lake Ontario and relaxing with friends and family. Mr. Thomas can be reached at:

1702 Empire Blvd. #4

Webster, NY 14580

twthomas@nrwcs.org

www.excelleratordj.com